REPORT DOCUMENTATION PAGE

Form Approved
OMB No. 0704-0188

1. AGENCY USE ONLY (Leave blank)	2. REPORT DATE	3. REPORT TYPE AND DATES COVERED
		FINAL

4. TITLE AND SUBTITLE
Five-Channel SQUID Based Non-Destructive Evluation (NDE) Instrument

5. FUNDING NUMBERS
61102F
1602/01

6. AUTHOR(S)
Dr Paulson

7. PERFORMING ORGANIZATION NAME(S) AND ADDRESS(ES)
Trintan Technologies

8. PERFORMING ORGANIZATION REPORT NUMBER
AFOSR-TR- 95 0142

9. SPONSORING MONITORING AGENCY NAME(S) AND ADDRESS(ES)
AFOSR/NE
110 Duncan Avenue Suite B115
Bolling AFB DC 20332-0001

10. SPONSORING MONITORING AGENCY REPORT NUMBER
F49620-92-C-0026

11. SUPPLEMENTARY NOTES

12a. DISTRIBUTION AVAILABILITY STATEMENT
APPROVED FOR PUBLIC RELEASE: DISTRIBUTION UNLIMITED

12b. DISTRIBUTION CODE

13. ABSTRACT (Maximum 200 words)

SEE FINAL REPORT ABSTRACT

14. SUBJECT TERMS			15. NUMBER OF PAGES
			16. PRICE CODE
17. SECURITY CLASSIFICATION OF REPORT	18. SECURITY CLASSIFICATION OF THIS PAGE	19. SECURITY CLASSIFICATION OF ABSTRACT	20. LIMITATION OF ABSTRACT
UNCLASSIFIED	UNCLASSIFIED	UNCLASSIFIED	UNCLASSIFIED

Tristan Technologies

Five-Channel SQUID Based Non-Destructive Evaluation (NDE) Instrument

F49620-92-C-0026

A 5-channel SQUID-based NDE instrument has been built and tested. A combination of first derivative axial and planar concentric gradiometers enable the simultaneous evaluation of magnetic signatures of surface and deep sources. Features of the system include: Liquid Helium dewar to cool the probe with 5 mm coil to external dewar surface distance, superconducting magnet assembly to provide both DC and AC applied fields, noise reduction circuitry to cancel signals generated by applied AC signals coupled to pick-up coils, computerized data acquisition and control system, including customized software, to control system, to collect, analyze and display data. Testing includes studies of transformation induced plasticity in steel, defects in non-magnetic metals using AC magnetic fields, defects in metals by applied modulated currents, AC fields applied to magnetic systems, and magnetization changes induced by applied tension. These tests indicate this system can locate and identify defects and sources in a variety of different applications using a number of novel experimental techniques.

(160 words of 200 max.)

Keywords:
SQUID, magnetometer, NDE (Non-Destructive Evaluation), multiple channel, noise cancellation, noise reduction, defects, superconducting

Table of Contents

List of Figures

1. Work Statement

The statement of work for this project is as follows:

I. Build a 5 channel SQUID-based NDE instrument that can be used for studying deep sources. It comprises the following elements:

- 5-Channel SQUID magnetometer probe with four, 5 mm diameter, 1st derivative axial pickup coils and one, 25 mm diameter, planar, concentric gradiometer.
- Liquid helium Dewar for use with the magnetometer probe and having a 5 mm spacing between the outer Dewar wall and the pickup coils.
- Superconducting magnet assembly on the probe capable of applying a 500 gauss DC field and 1 gauss AC field at a point 1 cm below the Dewar.
- Noise reduction circuit to cancel the applied AC field that is directly coupled to the magnetometer.
- Computerized data acquisition and control system to operate the SQUIDS, magnet assembly, and noise reduction circuit. Custom software will be written to perform these control functions, collect the data and analyze it to perform the experiments listed below.

II. Use the 5-channel system to perform the following studies:

- Identification of Flaws, Regions of Local Stress, and Precursors to Plastic Flow in Ferromagnetic Components.
- Clarify the microscopic mechanism responsible for the magnetic precursor to plastic flow in ferromagnetic materials.
- Determine how the magnetic precursor correlates with Barkhausen noise.
- Demonstrate the multiple-channel SQUIDs can localize the sites in the sample where individual stress-induced Barkhausen jumps are occurring.

III. Detection of Subsurface Flaws and Cracks, Such as Rolling Crack in Bearings for high-performance Aircraft.

- Determine whether high-resolution SQUID magnetometry can detect a precursor to either crack formation or the subsequent spallation from rolling contract in cylindrical test samples.
- Determine whether high-resolution SQUID magnetometry can allow nondestructive, quantitative observation of subsurface cracks, so that the factors governing the generation and growth of these cracks can be more readily determined.

2. Summary of Significant Accomplishments

The NDE system was designed and fabricated. A series of tests were conducted to examine the potential applications and sensitivities of the system.

As currently implemented, this system significantly exceeds the capabilities that were originally proposed. This is because we were able to identify several other companies that have an interest in applications of the type of equipment being constructed for the SBIR. They, in turn, specified and funded enhancements. These enhancements were then included in the NDE system at no cost to the program.

We have already shipped three systems that incorporate this technology and have orders to ship three more.

Some industrial applications that have assisted us in system enhancements include:

A manufacturer of Nuclear Fuel Rods.
A program with Vanderbilt University that is funded by a large US company.
A two year development program with a large Steel manufacturer.

Most of the enhancements were in the area of analysis software and noise reduction techniques. These will be discussed. Added features beyond the original proposal include a high speed data acquisition mode.

The current status of the 5 channel SQUID-based NDE instrument is as follows:

5- Channel SQUID magnetometer probe.
Constructed probe assembly with both planar and uniaxial gradiometer coil arrangements.

Liquid Helium Dewar
The Dewar has been fabricated and tested.

Superconducting magnet assembly.
Design and construction of the magnet assembly is complete.

Noise reduction circuit.
The noise canceling unit (NCU) has been completed and is operational.

Computerized data acquisition and control system.
Software has been developed and is now capable of acquisition and control of up to 8 SQUID channels with up to 8,000 data points per block. Maximum acquisition rate is 250 Hz. Graphics capabilities include generation of 3D and 2D plots of a scanned surface. Have also implemented a high speed data acquisition mode.
The Scanner table subsystem has been constructed and is working properly.

Tests of System Capabilities
A series of tests have been conducted to demonstrate experimental techniques that may be used to exploit the capabilities of the system. These have shown the sensitivities that may be expected, and indicate a number of avenues for further development.

2.1. System Description

The main components of the system are:

- Five-Channel SQUID Magnetometer Probe
- Liquid Helium Dewar

- DC and AC Magnet System
- AC Nulling System
- Computer Control and Data Acquisition System

These components are connected to form the NDE system as shown in Figure 1.

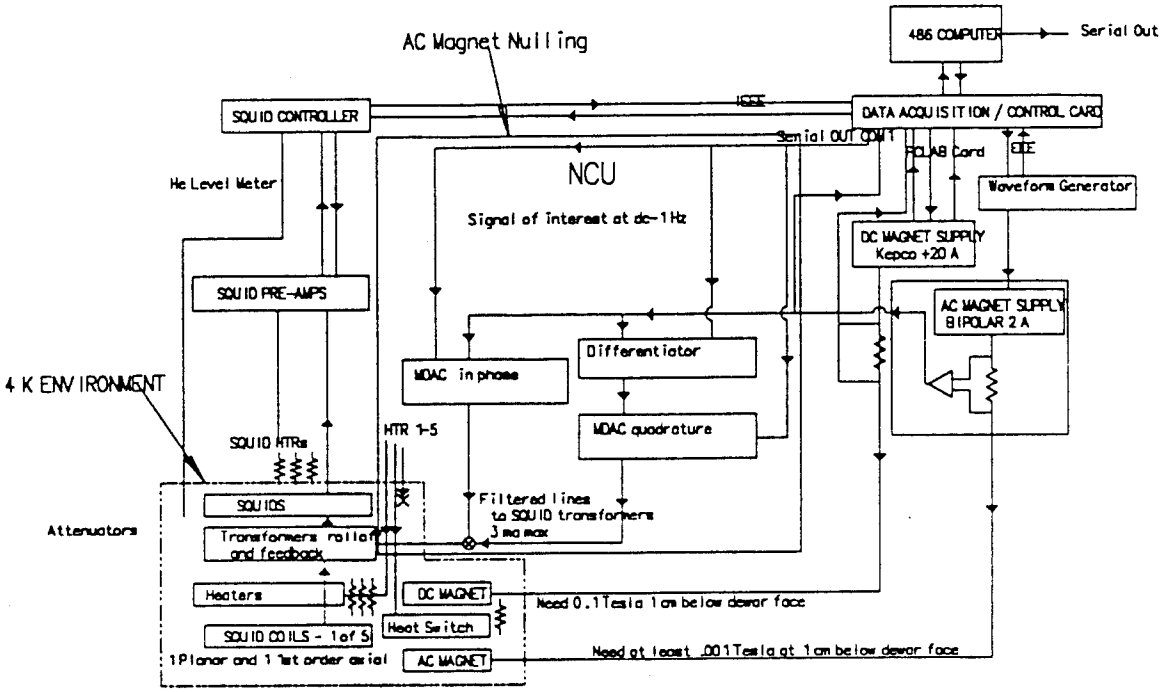

Figure 1: System block diagram

2.1.1. Five Channel SQUID Magnetometer Probe

An engineering drawing of the Magnetometer Probe is shown in Figure 2.

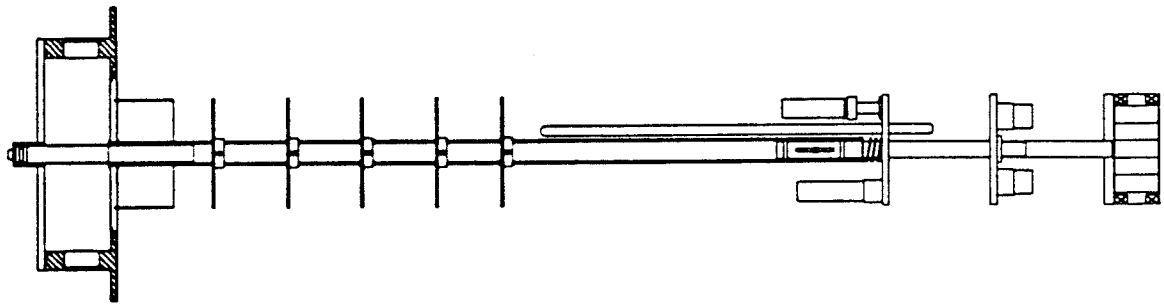

Figure 2: Magnetometer Probe Drawing

The SQUID input coils are constructed entirely of low temperature superconducting materials. The entire input loop is superconducting with a roll-off of about 1 KHz. The inputs have a spatial sensitivity as shown below in Figures 3 and 4.

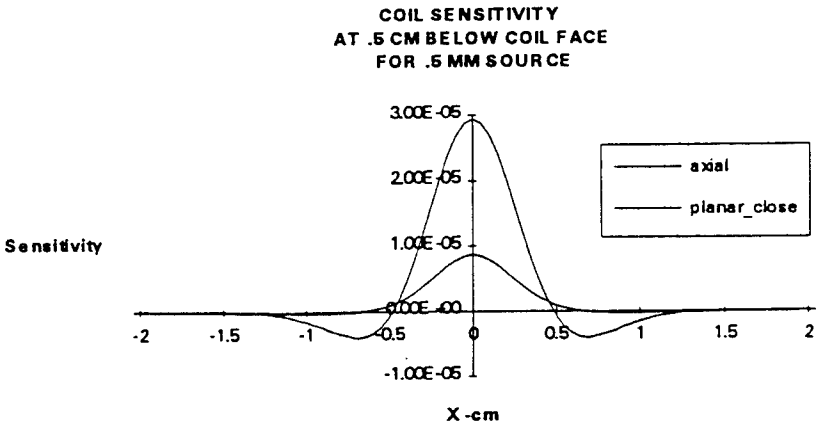

Figure 3: Detector Coil Sensitivity 0.5 cm below coil face.

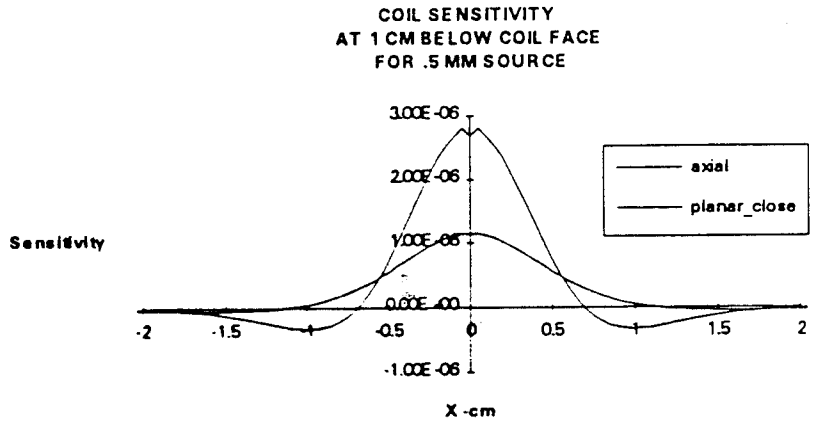

Figure 4: Detector Coil Sensitivity 1.0 cm below coil face.

2.1.2. Liquid Helium Dewar

An engineering sketch of the Liquid Helium Dewar that has been fabricated to hold the magnetometer probe is shown in Figure 5.

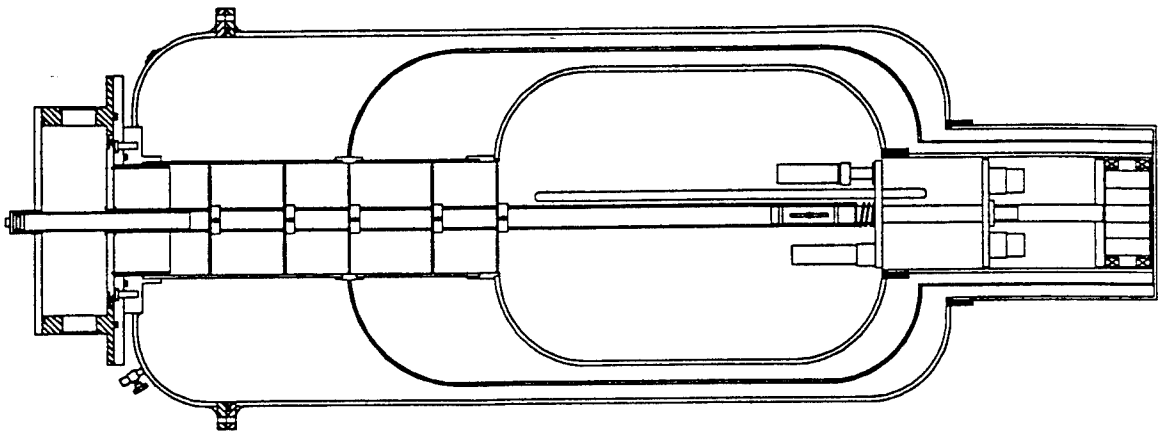

SBIR 2007-001

Figure 5: Liquid Helium Dewar

2.1.3. D.C. and A.C. Magnet System

D.C. Field System

The superconducting magnet on the magnetometer probe will be capable of applying a 0.2 Tesla D.C. magnetic field to a sample located below the bottom of the Dewar. The D.C. magnet operates in a persistent field mode.

Power supplies are provided to operate both the magnet current and persistent switch heater. The switch heater, D.C. current amplitude, and ramp rate are all controllable from the computer. (The operator may be required to turn the power on to the D.C. supply prior to changing the field and the software will warn the user as necessary).

The D.C. magnet is 2.4 cm in diameter and 0.9 cm long. The measured field profile from this magnet is shown in Figure 6.

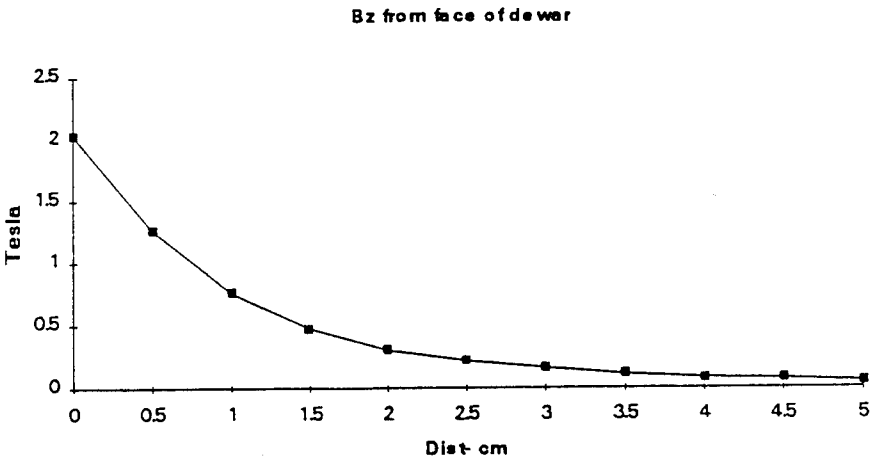

Figure 6: Magnetic Field as a function of distance along the axis.

A.C. Field

An A.C. field of amplitude 0.0002 Tesla below the bottom of the Dewar may be produced. This magnet will be operated in the persistent mode to maintain the D.C. field simultaneously with the A.C. field; the A.C. field will be produced by inductive coupling of flux into the magnet circuit. The circuit is shown in Figure 7. A power supply is provided to generate the A.C. field under computer control. The amplitude and frequency of the A.C. field is adjustable using the computer control system.

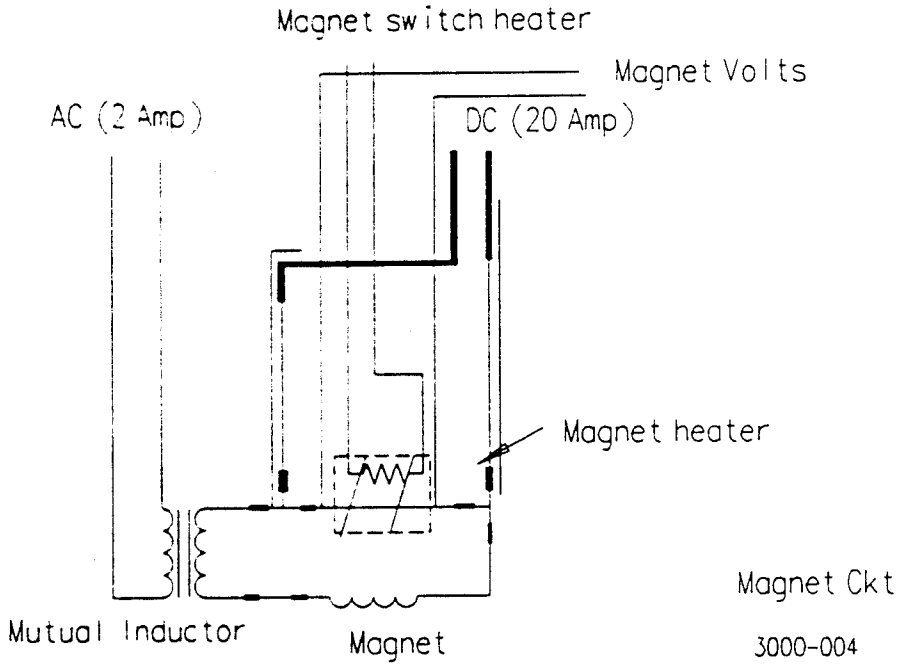

Figure 7: Superconducting magnetic field circuit.

2.1.4. A.C. Nulling System

A custom designed A.C. nulling circuit will supplied in order to cancel A.C. flux from the A.C. magnet that is coupled into the input circuits. This circuit is shown schematically in Figure 8.

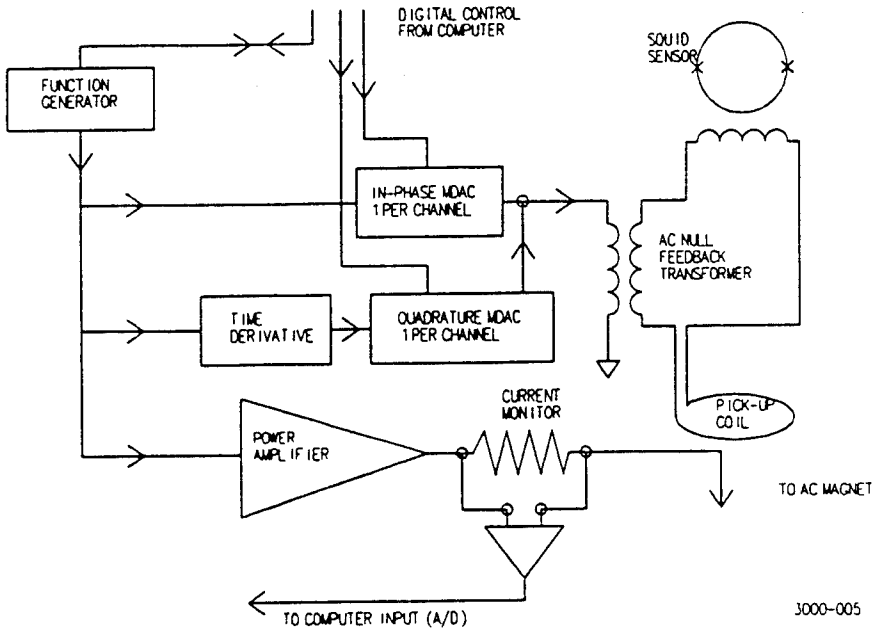

Figure 8: A.C. Nulling block diagram.

Since the gradiometers can not be perfectly balanced, a large A.C. signal will be directly coupled into the system whenever the A.C. magnet is used. Even if the magnetometers are perfectly designed and manufactured, a large A.C. signal would still be directly coupled to the pick up coils due to the radial gradient of the applied A.C. field. Although we could design the coils to reject this gradient, the coils would then not work so well to reject other magnetic noise. Furthermore, placing a metal object under the magnetometer would seriously degrade this rejection capability.

The directly coupled A.C. flux detected by the gradiometer is between 1% and 5% of the flux that would be detected by a magnetometer of the same size. This results in an extremely large A.C. signal which is independent of the sample. In most cases, this signal will be so large that it will be nearly impossible to analyze the data to detect flaws.

With a carbon steel sample under the system, we expect that the A.C. flux detected by the gradiometer will many times larger than the signal which would be detected by a magnetometer if no sample were present. The dynamic range of the data acquisition system will not be adequate to track this large signal while still resolving the small signal from defects in the metal.

To minimize this problem, we will require an A.C. magnet nulling system. This system consists of the following items:

- Special circuitry to generate in-phase and quadrature feedback signals to null the A.C. signal in the SQUID. This circuitry will receive an analog input from the magnet power supply and digital input from the computer. The computer input will adjust the amplitude of the in-phase and quadrature signal used to separately null the A.C. signal on all SQUID magnetometer channels.
- All necessary modifications to the magnetometer probe and SQUID electronics allow injection of the A.C. null signal directly into the input circuit.

- Software to automatically optimize the feedback signal. When the operator issues a single command, the computer will automatically analyze the data from the magnetometer and feed back the appropriate signals to null the A.C. output. Software will allow manual adjustment of this null.

This system is capable to null A.C. signals of any amplitude up to the full scale ± 5 Volts p-p output of the SQUID magnetometers when operated on range x500. The nulling circuit has at least 12 bits of resolution which will result in a maximum A.C. output after null of less than 2 mV rms for a full scale output from the SQUID magnetometer.

Provision is made to switch the full scale feedback signal to be 10 times the full output of the magnetometers. This allows the operator to adjust the null signal with a low level A.C. field and then turn up the A.C. field amplitude signal to an amplitude which would otherwise have caused an overload of the SQUID.

We expect that the quadrature null will usually be used when applying A.C. magnetic fields to conductors. With this A.C. MAGNET NULLING option, it will be possible to null the magnetometer output after placing the sample under the system. Any defects in the test sample will then show up as large changes in the A.C. output of the system as the sample is scanned under the magnetometer. Since the null can be set quickly and automatically by computer, we expect that it should be done every time a new sample is placed under the magnetometer.

Noise Cancellation Unit (NCU)

The Noise Cancellation Unit has been fabricated by Tristan Technologies, Inc. and includes the room temperature electronic circuits required to perform the A.C. magnet nulling function. It also provides miscellaneous other circuits such as: 1) Relays to turn SQUID heaters on or off, 2)control relays for various switching applications, and an A.C. magnet current output. The major sections of the circuit are shown in block diagram below.

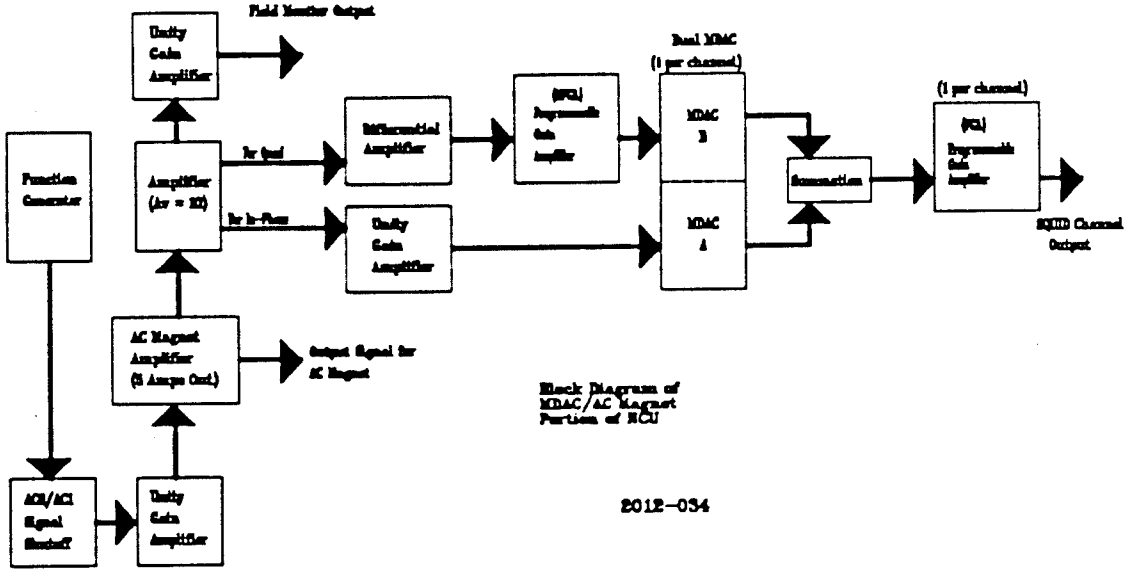

Figure 9: NCU MDAC/A.C. magnet Block Diagram

2.1.5. Computer Control and Data Acquisition

All of the system Data Acquisition electronics and the computer control system will be housed in a custom-fabricated control console. This console is desk-like in nature and will be approximately 1.5 m wide by 0.6 m deep by 0.7 m tall. A single power cable from this console provides A.C. mains power to all necessary components in this system.

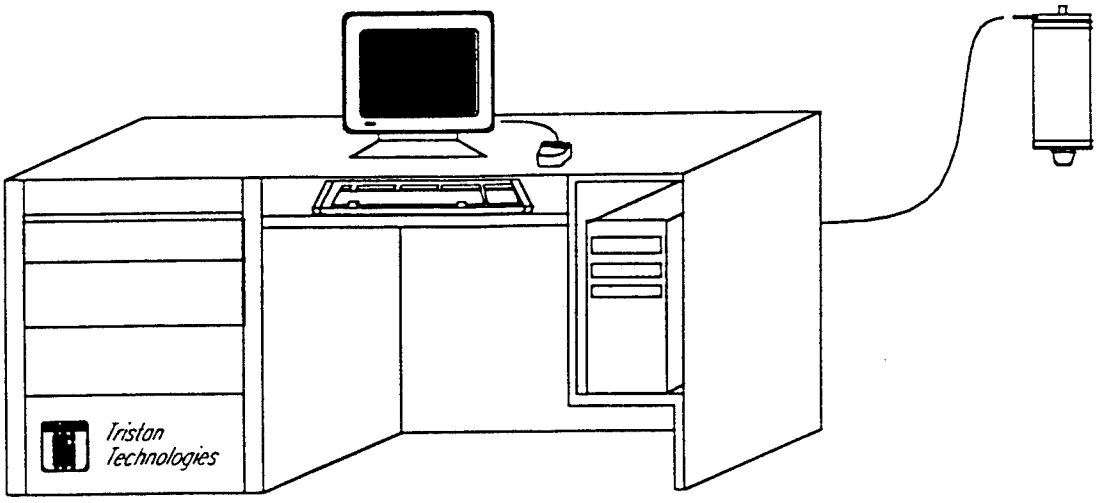

Figure 10: Superconducting magnetic field circuit.

The NDE system is controlled by an IBM-AT compatible computer system mounted within the control console. This equipment includes:

- 80486 microprocessor
- Color monitor
- Mouse and keyboard
- 4 MByte memory
- 200MByte hard disk
- One 5.25" floppy (1.2 MByte)
- One 3.5" floppy (1.44 MByte)
- Combination Analog and Digital I/O card.
- IEEE-488 compatible digital communication card
- Two, RS-232 communication ports
- One, Centronics compatible, 8 bit parallel port
- One, cartridge tape back up (120 MByte compressed capacity)
- MS DOS 5.0 operating system
- National Instruments Lab Windows Software

Software is being developed that will perform data acquisition from all SQUID channels, control of all system components, and analyzing the data to determine the magnetic properties of the sample being tested.

Some specific features include:

A.C. Field Control

Both amplitude and frequency of the sinusoidal, A.C. field applied to the sample are computer controlled. In addition we have provide for a DC offset current to be set. The field is automatically turned on and off as required during specific measurements.

D.C. Field Control

The D.C. field amplitude and ramp rate is computer controlled. A fully automated routine operates the heat switches and ramps the field as required.

SQUID Control

All necessary functions of the SQUID system are under computer control via the IEEE-488 bus. Utilities is provided to allow direct operator control of:

- SQUID Gain
- SQUID Reset
- Range
- SQUID Heaters

These, and many other SQUID control functions, are automatically controlled as required to perform various sample measurements. In particular, all necessary data acquisition parameters are automatically set by the computer prior to a sample measurement.

Heater Control

The magnet persistent switch heater, SQUID heater, and pick up coil heaters are operable from the computer console. These heaters are also automatically switched on and off as required for various sample measurement procedures.

Interface to Automated Motion Control

The system is capable of interfacing to an automated magnetometer positioning mechanism. Communication between the positioning mechanism and the data acquisition computer will coordinate the motion to the acquisition of data.

AC Signal Nulling

Complete control of the A.C. Field Nulling Circuit allows the operator to manually null the in-phase and quadrature signal from the A.C. magnet that is detected by each SQUID channel. An automated procedure is also supplied that automatically nulls the signal from all channels by issuing a single command prior to data acquisition.

Automated Data Acquisition Procedures

Three classes of automated data acquisition procedures are planned:

- Manual Trigger Mode; where the operator will trigger each burst of data using the computer mouse.
- Timed Mode; where each burst of data will begin after a predetermined delay time until all bursts specified have been acquired.
- Remote Trigger Mode where each burst of data will be triggered by a remote signal. This will usually be used to synchronize data Acquisition with the scanning device.

In each mode, the operator is prompted to specify:

- Channels from which data is to be acquired.
- Data acquisition rate (samples/sec).
- Number of data points to be acquired in a single burst.
- AC field amplitude and frequency.

If the operator desires, and the acquisition rate is slow enough to allow for it, the operator will be able to view the acquired data in real time on the CRT monitor.

High Speed Data Acquisition Mode

A high speed data acquisition mode has been incorporated. In this mode, data can be acquired at 24 kHz, and analyzed in real time, thus saving the necessity of storing large quantities of data off-line and analyzing later. In-phase, quadrature, and amplitude data is saved. The data

acquisition rate may be spread to as many channels as are desired or are available, but the total acquisition rate should not exceed 24 kHz.

Data Analysis Functions

After the data has been acquired and stored in a file, the operator is able to process the data using a variety of data analysis functions.

All data that is acquired is stored in a standard format that will include a header file describing all of the important data acquisition parameters. A new file will be created by the data analysis function that has the same format as the original file. The header file will be modified to indicate that the data has been processed by the specified data analysis function.

Several data analysis functions will be required. Currently planned functions include:

- Decimate - This reduces the number of data points stored in the file by rejecting a specified percentage of the data points. A specified number of points at the beginning and end of each data burst can also be rejected.
- FFT -A fast Fourier transform will be applied to each burst of data.
- Average - This averages the data over a specified parameter, e.g. the data from all bursts in the file could be averaged together or multiple FFT's could be averaged together.
- B/H Slope - Calculate the ratio of change in magnetometer output to change in applied field. This ratio can be calculated for each cycle of applied A.C. field or for the average of all cycles of applied field during the data burst.
- B/H Area - Calculate the area of the B/H loop. This can be done for each cycle of applied field or for the average of all cycles.
- Amplitude - Calculate the peak-to-peak amplitude of the magnetometer output (or any other measured output) during a single cycle of applied A.C. field or during a single burst of data.
- Filter - This applies a low-pass, high-pass, or band pass digital filter to the data.

Data Plotting Functions

A variety of data plotting functions will be required in order to operate on the standard data format. This will allow any data file to be plotted in any of the following formats (some of these formats may not be meaningful for some of the data files).

- Time Series - Plots the data amplitude versus data point
- X-Y Plot - Plots the amplitude of one magnetometer function versus A.C. current.
- Contour Plot - Plots the amplitude as a contour plot versus X-Y position.
- 3-D Contour Plot - Plots the amplitude of a data set versus X-Y position.

2.2. Discussion of Testing Techniques and Results

2.2.1. Magnetic Studies of Transformation Induced Plasticity in Steel

In the late 1960's researchers at UC Berkeley developed a variety of steel alloys which undergo a phase transformation from an austenitic to a martensitic phase under strain. The latter has greater plasticity, and the idea was for this induced phase transition to relieve built-up local stresses thereby yielding a class of materials which react favorably under conditions of stress. This class of steels is referred to as TRIP (Transformation Induced Plasticity) steels.

We contacted Dr. Bruce Westermo (Civil/Mechanical Eng., SDSU) and Dr. Larry Thompson (Mech. Eng., SDSU), co-owners of Strain Monitor Systems (SMS) of San Diego. SMS are exploiting the magnetic change associated with the TRIP steel strain induced transformation to produce strain monitors. They provided us with a series of strained and unstrained samples for testing.

Trip steel undergoes a transformation from austenitic (FCC and relatively non-magnetic) to martensitic (BCC and magnetic). This system provides a good starting point for using the NDE system to study the plastic flow by magnetic means. Additionally, this material appropriately configured can be used as a strain monitor with a magnetic detection scheme of the strain. Given the sensitivity of SQUID magnetometers, the potential exists to place the monitors remotely (e.g., within bridges, buildings or other hard to access locations) and detect the induced strain with appropriately configured and placed magnetometers.

A series of strained samples are shown is Figure 11. The samples are 0.007" thick. The strain percentages reflect the peak strain applied as measured by a strain meter and do not account for subsequent relaxation or strain meter compliance. The strain as dimensionally measured post-strain is about 2/3 the indicated values.

For all the samples discussed, the straining was performed in ambient magnetic field and a zero applied field measurement was taken of them in the as-strained state. Subsequently, the samples were magnetized with a permanent magnet and then measured in a zero field environment. Two different types of measurements were taken - a 2-D scan of the sample covering an area of 8 x 12 cm with the sample approximately centered with the long axis in the 12 cm direction, and a single linear scan along the sample length (used as a monitor or relative measurement of the sample).

Figure 12 is a surface plot showing the DC Squid output as the sample is rastered 0.31" below the dewar tail. A 1 kHz SELS filter is used on the SQUID output, and the DC value is the average of 1200 measurements taken at 1200 Hz. The scan stepsize is 0.25 cm, for a total of 1617 points. The signal is very strong, and there is little need for such averaging as the data indicates. These parameters are representative of all the scans taken here. In Figure 12, the sample is the 25% strained sample in the as-strained state (no external magnetic field other than the earth's has been applied). The multiple peaks indicate that the sample has multiple domains and is not well-aligned. The peak height is less than 15V.

Figure 13 shows the same scan following the magnetization of the sample (by pulling a permanent magnet along the length of the sample). We note that there is now a single positive peak and a corresponding negative peak as one might expect from a magnetized, well-aligned sample. Also, we note that the peak magnitude is now over 150V, a more than 10-fold increase.

Figures 14 through 17 show similar scans of the 15%, 10%, 5%, and unstrained samples respectively in the post-magnetized state. It is observed that there is a steady decrease in the peak amplitudes, and that the 2-lobed response seen in Figure 13 begins to break into an additional set of peaks. This is interpreted as the formation of multi-domains because the field energy begins to dominate the exchange coupling between the magnetic regions.

Scans along the axis of all the samples in their as-strained unmagnetized state are shown in Figure 18. They show multiple peaks and magnitudes of order 10V. This points to the importance of applying an external field to the samples to both maximize the signal and to distinguish the strained and unstrained materials. Following magnetization, the same scans are repeated with markedly different results as seen in Figure 19. There are now much larger signals, by roughly an order of magnitude, and there is a clear correspondence between strain and peak amplitude. There is also a clear relationship between the induced strain and the ability of the sample to maintain a well-aligned magnetization, with the more strained samples showing a greater propensity to align. The peak to peak signal strength versus strain relationship is shown in Figure 20. The smooth monotonic relationship encourages one to believe these devices can be calibrated to give additional quantitative information.

A horizontal pick-coil is sensitive to components of magnetization both in-plane and perpendicular, although the response functions are slightly different. Two samples (0% and 15% strains) were scanned along the central axis, then flipped 180 degrees about that axis, and the scan repeated. By symmetry, magnetization along the axis should produce the same result, thus differences between the two can be

interpreted as off-axis magnetization. These are shown in Figure 21 with difference curves in blue. Lobes are seen at either end for both samples, but a relatively small difference curve is seen near the center of the 15% sample indicating largely axial magnetization, whereas a larger difference curve is seen in the center region for the 0% sample where multi-domain structure indicates rotation of the magnetization.

Figure 22 demonstrates that the signals are easily detected through intervening materials as indicated.

A 2-D spectral plot of the data from Figure 17 is displayed in Figure 23 to reveal the multi-domain magnetization has transverse in-plane components.

2.2.2. Studies of Defects in non-magnetic metals

Studies were undertaken to demonstrate various techniques for detecting and locating defects in non-magnetic metals. In one set of measurements, an external AC magnetic field is applied to the metal. Eddy currents set in motion by these fields generate magnetic fields that are picked up by magnetometer. Defects disturb the normal eddy current patterns, and these changes can be detected and used to locate and characterize the defect. In the second set of experiments an electrical current is passed through the specimen and the magnetic field created reflects the current distribution around defects. The current is modulated and lock-in detection employed to enhance the signal detection.

Sensitivity to Eddy Currents Generated by the Probe AC Magnet

A series of tests were conducted to determine the experimental parameters that optimize the sensitivity of the system to metal voids. These parameters include the AC magnet frequency, the driving current, and the resulting lock-in phase shift. This was done by a series of scans across the edge of 1/2" Al plate. Although the frequency is varied, a one second data collection time at each location was adopted, so as to optimize with respect to a fixed data collection time. The Al plate - tail distance is fixed at 0.125", a 6 kHz data acquisition rate per channel is used, with a SELS filter of 4 kHz. For all the data, the NCU is used to null the signal while located over the Al plate. The high-speed data acquisition mode is used, and we obtain both in-phase and quadrature responses.

Figure 24 shows the in-phase response as 8 cm. scans across the Al edge is performed. The Al edge is located at approximately the 0 cm. position. The AC frequency is 4 Hz., and at a series of AC magnet currents from 0.2 amps to 5 amps. There is no discernible evidence of the Al edge. Instead we observe that the higher currents yield significantly larger drifts. Figure 25 shows the quadrature responses for the same series of scans. Of course we expect the eddy currents to be a maximum where the field is changing most rapidly, 90 degrees from the field maximum. Although the driving frequency is low, there is clearly evidence of the Al edge even at the lowest current setting. The magnitude of the change is proportional to the current, and this constant of proportionality is measured to be 1.6 V/A.

Figures 26 and 27 show the same series of scans at 12 Hz. It is now seen that there is definite in-phase response, although considerably less than the quad. Again, the drift and noise is apparent at the higher current settings. The drift is not so apparent in the quad as the that signal is much larger than the drift.

Repeating a series of similar scans at 40 Hz reveals a proportionally greater degree of in-phase signal, as well a greater response signal overall (Figures 28 and 29). Indications are that the maximum response is phase shifted at higher frequencies. At 40 Hz. the response/current proportionality constant is 10.1 V/A for the quad response. Data was also taken at 24 Hz, but is not shown here.

The phase shift or rotation angle of the response can be calculated, and is shown in Figure 30, along with the quad and in-phase response sensitivities versus frequency. The response magnitude is seen to be reasonably linear at low frequencies, with roll-off above 24 Hz. A useful operating point for this type of detection is 24 Hz and 1 amp driving current. At 24 Hz, the quad response is still largely dominate.

Cylindrical Holes in Al

A 3/8" Al plate was drilled with a series of cylindrical holes. The diameters were 1/8", 1/4", and 3/8". Additionally, these were drilled to depths of 1/8', 1/4", and 3/8" to yield a total of 9 holes. The holes were spaced on a 1 1/2" square lattice. A 12 x 12 cm. scan with .25 cm. steps was taken, using a 1 amp AC current at 24 Hz to drive the magnet.

Shown in Figure 31 is the quad response from this scan. In this image, we see only 6 of the holes. Along the x=0 cm. line are two 1/4" diameter holes, with the 1/4" deep hole at y=3cm, and the 1/8" deep hole at about y=1. The two 3/8" diameter holes are along the x=4.5 cm position, with the depths and locations the same as for the 1/4" holes. Along x=-3.5 cm. lines are two 1/8" diameter holes, again with depths and locations the same as for the 1/4" holes. The latter two holes are just barely discernible. The other 4 holes can be seen much easier. While the Al edges are outside this image area, they are the most discernible features, far exceeding the signal magnitudes of any of the holes. As will be seen later, the circular shape of these defects are less effective generating these signals than are straight edges, and this is in part responsible for the difference in response.

Figure 32 shows the in-phase portion of the scan. The holes are less discernible as expected, although at 24 Hz there is sufficient in-phase response to show them. Figure 33 shows the center hole (1/4" x 1/4" deep) for both the in-phase and quad response in greater detail.

Quantitative Measurements of System Sensitivity to Metal Cracks

To simulate and calibrate the sensitivity of this method to cracks in the metal, various grooves were cut into the surface of an Al plate and linear scans across them were made. Initially it was observed that butting two similar plates against each other underneath the probe gave a strong signal that was relatively unaffected as the plates were separated by moderate distances (less than 1 cm.). This indicates that the area of cracks is more important than the volume. Additionally, it is expected that the shape of the defect relative the applied magnetic field profile is important and configuring the field will allow for further optimization of signal detection relative specific types of defects.

The grooves were cut into a 1/2" Al plate to depths of 1/16", 1/8", and 1/4". The widths were uniformly 0.18". Scans were conducted using experimental parameters as above except where noted. Figure 34 shows scans across these three grooves. The left edge of the Al is at approximately -3 cm. on this scale and the right is at +19 cm. There is relatively little gained by averaging for 6 sec. as opposed to 1 sec. The 6 sec. avg. time was adopted to allow for adequate data acquisition time at slower AC frequencies. Also shown are results for 12 Hz and 6 Hz. In all the scans the location of the three grooves are apparent, with the greater sensitivity occurring at higher frequency and for deeper cuts.

By flipping the plate over, the grooves are located in the bottom surface and we can attempt to locate the grooves again. Shown in Figure 35 are these results (included for comparison is a front side scan on a separate scale). Only the 1/4" cut is readily apparent for any of the three frequencies shown. In large part the reduced sensitivity is due to the increased distance of the groove from the tail of the probe.

The amplitudes of the quad response versus groove depth and frequency are shown in Figure 36. There is a high degree of linearity of the response versus groove depth. Noting from Figure 34 that the full width half max. is approximately 2.5 cm., it is reasonable to assume an effective crack area for the 1/4" groove of 1.6 cm^2. This gives a sensitivity of about 1 V/cm^2 (at 24 Hz, tail distance of 0.100", and 1 amp AC magnet current). In comparison, the round 1/4" x 1/4" deep hole (for an effective area of 0.4 cm^2) gives a sensitivity of only about 0.37 V/cm^2.

2.2.3. Detection of Simulated Defects by Modulated Current

Another technique for detecting defects in metals is to run a current through the metal and to detect disturbances in the current distribution via the magnetometer. To enhance the sensitivity and to remove other environmental magnetic signals from interfering, this can be done with an AC current. A metal plate of 1/4" thickness, 4" wide, and 18" long had a several slots cut into it. The individual slots were

well-separated to isolate each other. The first slot was cut through the plate, and had a length of 1" and a width of 1/8". The length of the slot is parallel with the plate width. Shown in Figure 37 is a 3-D surface plot generated by a 2-D scan using a 1 amp, 12 Hz AC current running parallel to length of the plate. The plate edges as well as the slot are quite easily seen. As expected, the signal here is in-phase.

Cutting a similar slot, but this time oriented along the length of the plate produces the image in Figure 38. Clearly the signal from the presence of the slot is significantly reduced, showing the sensitivity of this technique to the orientation of anisotropic defects.

A third slot was cut similar to the first, but only to a depth of 1/8". Figure 39 shows the results from a scan of this slot. Again, the experimental parameters are the usual ones, and we note that the signal from the slot is significantly reduced from the amplitude seen from the first slot. One may assume the current is pushed down as well as out toward the edges, resulting in less than proportional signal reduction. Finally, the plate is flipped over and the same scan of the last hole repeated. Although some reduction in the amplitude of the signal is seen, this can be attributed to a tail-sample distance effect.

2.2.4. Magnetic Sensitivity to Modulated Wire Currents

As evidenced by the above data, the system is quite sensitive to currents. The minimum detectable current using this system then sets the lower limit on the sensitivity this technique offers. A 0.003" Cu wire was placed below the tail at a distance of 0.100". Small AC currents were passed through the wire, and the usual lock-in technique was used to detect magnetic fields generated by the current. Because the AC magnet is not in use, there is no use for the MDAC functionality of the system. The MDAC were disconnected and the following measurements were taken. A driving frequency of 12 Hz was adopted, and a resistor network used to divide down the current provided by the AC magnet current source. As we have conventionally done, a 1 second data acquisition time per scan point is used. Figure 42 shows the signal from a scan across the wire carrying 10 micro-amps. The S/N ratio here is roughly 10, thus the lower limit is about 1 micro-amp. Obviously, additional measures might be taken to improve this.

In Figure 43 are two high S/N scans from 200 micro-amp currents at 12 and 25 Hz. There is little difference between the two. We did note some quad signal (of about 1/20 at 25 Hz), and at lower frequencies one can begin to expect 1/f noise problems.

2.2.5. Quasi-magnetic System under Modulated Field

Stainless steel is not normally considered a magnetic material, but it does have sufficient magnetic susceptibility to allow imaging by exciting by an externally applied magnetic field. Shown in Figure 44 is an image from a 3/8" stainless steel plate. In the plate are four holes of 3/8", 5/16", 3/16", and 1/8" diameters. All four peaks can be seen although the smallest is just noticeable.

2.2.6. Tension Induced Magnetization Changes in Fe

Magnetostriction effects are another potential use of the NDE system. A 0.007" Fe wire was put under tension and scanned by the probe. Because the expected magnetostrictive changes were expected to be small, an AC method was used. The AC magnet current supply was disconnected from the probe and used to drive a linear motor. The linear motor provides a linear motion that is proportional to the applied current. Thus it may also be used to apply tension to the Fe wire and, when driven by a relatively slow AC current, will apply an AC tension. The response signal is lock-in detected using the driving current as a reference. Additionally, because the AC magnet supply can be programmed to oscillate about a DC offset, this AC tension may be on top of a DC tension. In setting up the experimental arrangement, it was necessary to pre-tension the wire, so that a DC offset of 0 does not correspond to no applied tension.

A particular problem that plagues this kind of measurement is the possibility of movement of the wire as tension is applied. Because the magnetization of the Fe wire is extremely large and varies along the length of the wire, even small movements can induce false signals.

Shown in Figure 45 are a series of 5 scans laterally across the Fe wire under different DC offset tensions. It is seen that the signal maximum, directly above the Fe wire, varies with the DC offset. It initially increases, goes through a maximum and then decreases. Recall that a zero offset does not imply 0 applied tension; in fact, there is significant tension as the Fe wire was pre-loaded. Thus we do not expect the curve to extrapolate to zero. Limited throw of the linear motor prevented offsets above 0.8 Amps.

Iron is known to undergo Villari reversal, where the magnetization change with applied tension reverses direction. This may be a demonstration of that, though one is cautioned against drawing that conclusion from this data alone. Magnetostriction has been used to measure crack lengths in low alloy steels employing a voltage potential drop technique in conjunction with cyclic loading (see F.H. Davis and W.J. Plumbridge, "Magnetostriction Effects in Crack Length Measurements ", Fatigue, Fract. Engng. Mater. Struct., Vol. 11, No. 4, pp 241). In part, the technique relies on the magnetostrictive behavior of the alloy. It may be possible to combine the sensitivity of the NDE magnetometer and cyclic loading or stressing to examine defects or defect growth.

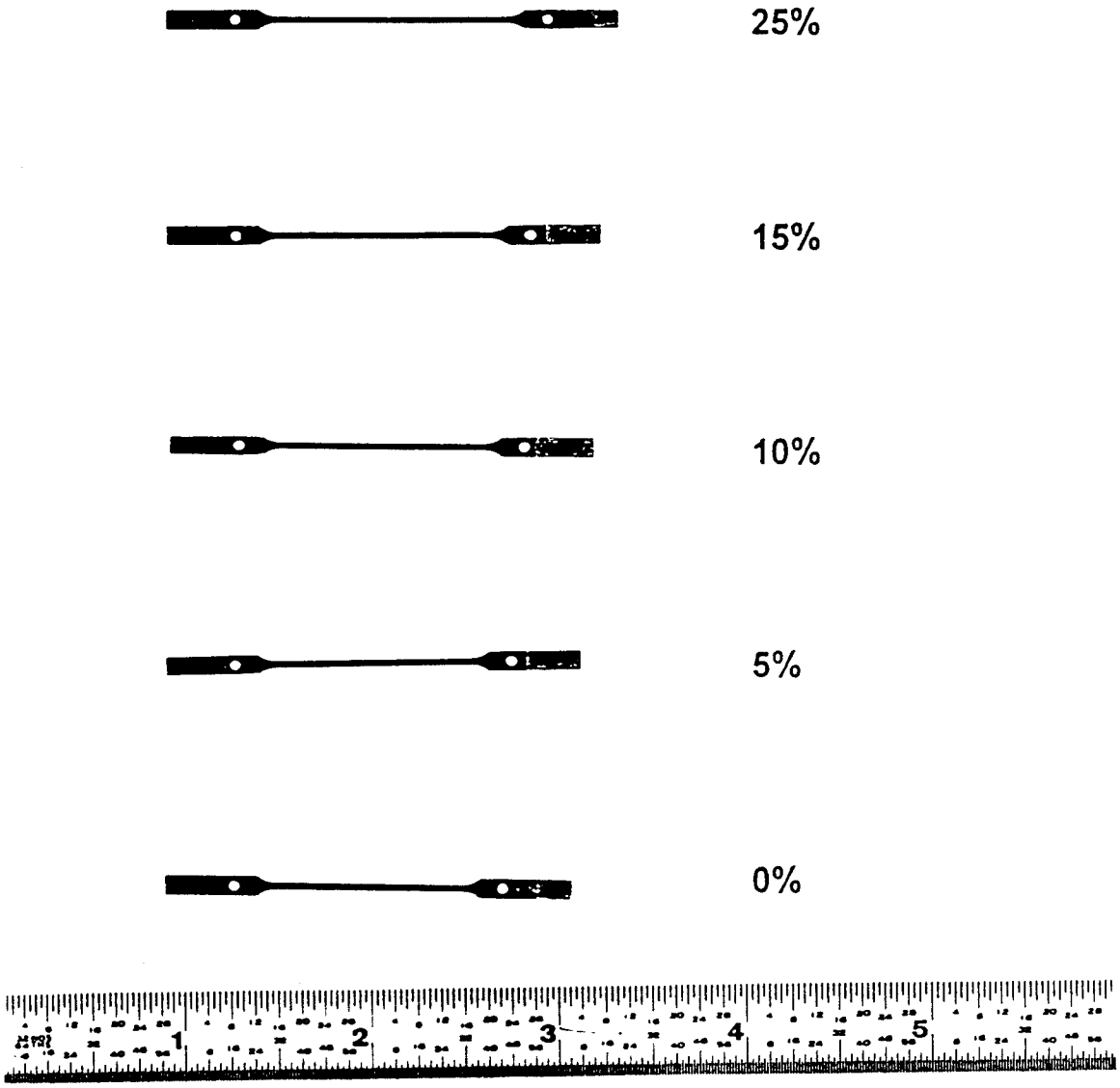

Figure 11 The TRIP steel samples are shown with the corresponding percentage strain. The strain percentages reflect the peak applied strain and do not account for relaxation of the sample or strain meter compliance.

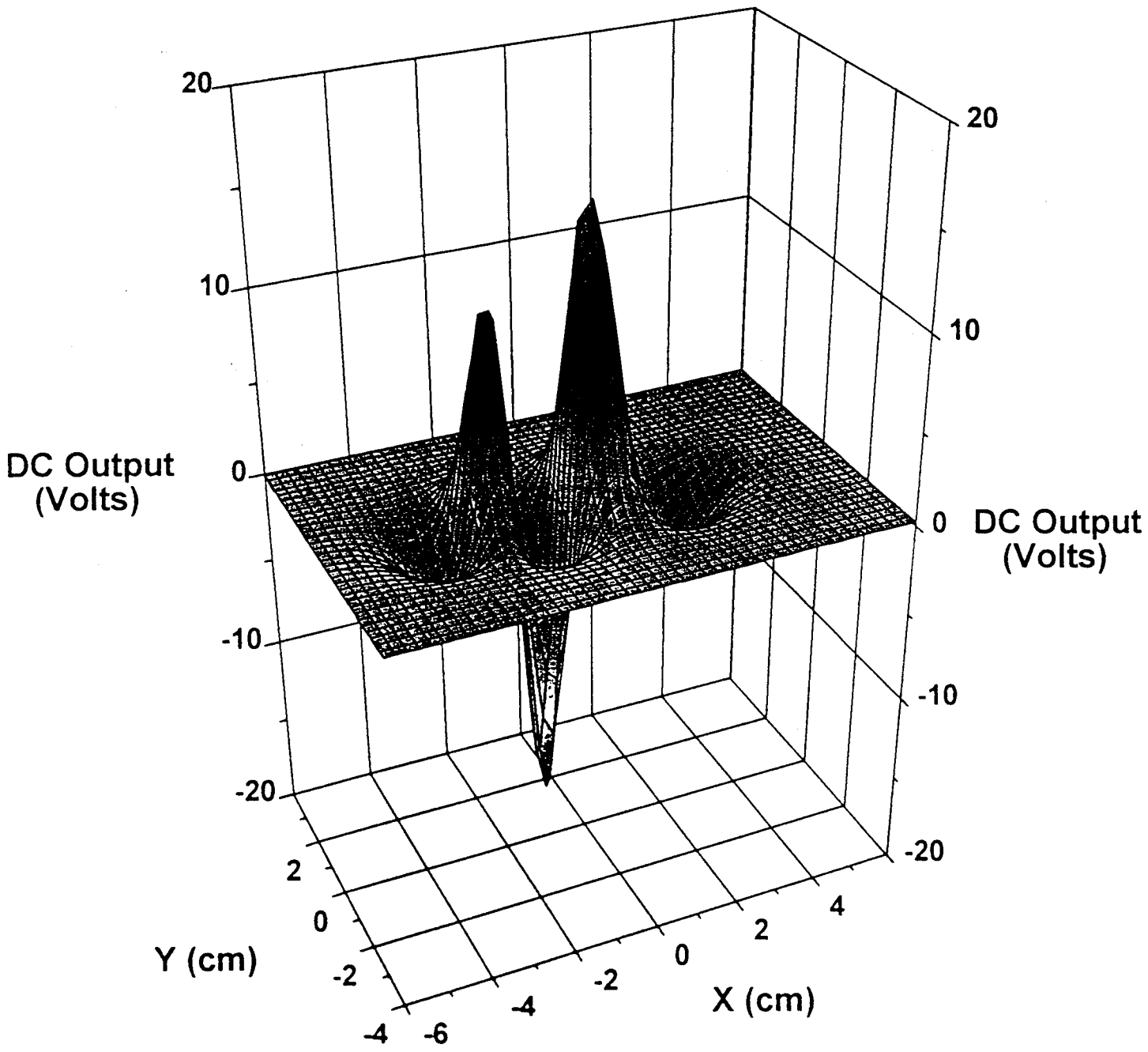

Figure 1. Image of the 25% strained TRIP steel in the as-strained state.

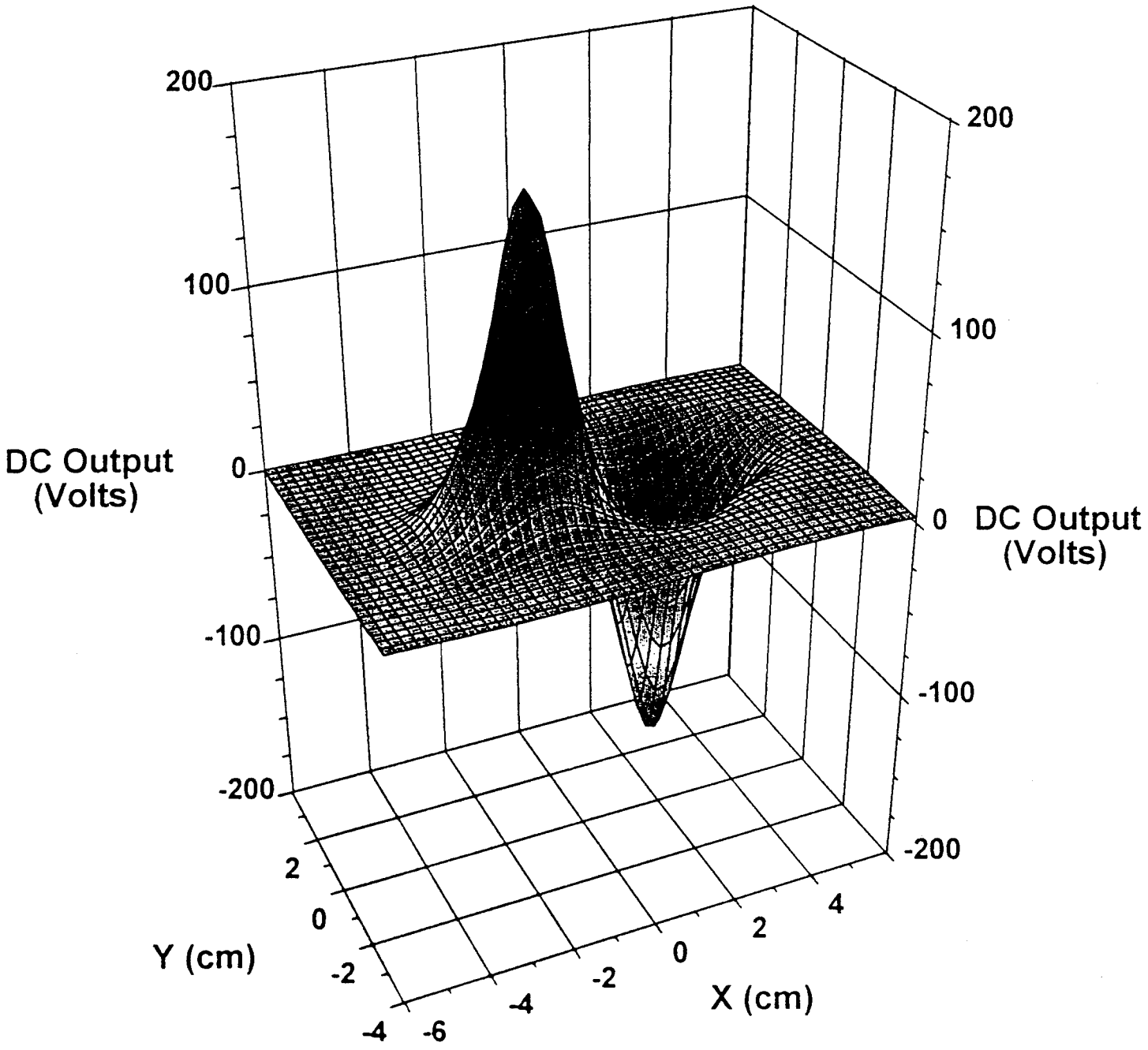

13

Figure 2. Magnetic image of a 25% strained TRIP steel sample in the post-magnetized remanent state as generated by x-y scan using a uniaxial gradiometer. The gradiometer is run in DC mode with no applied magnetic field and a tail to sample distance of 8 mm.

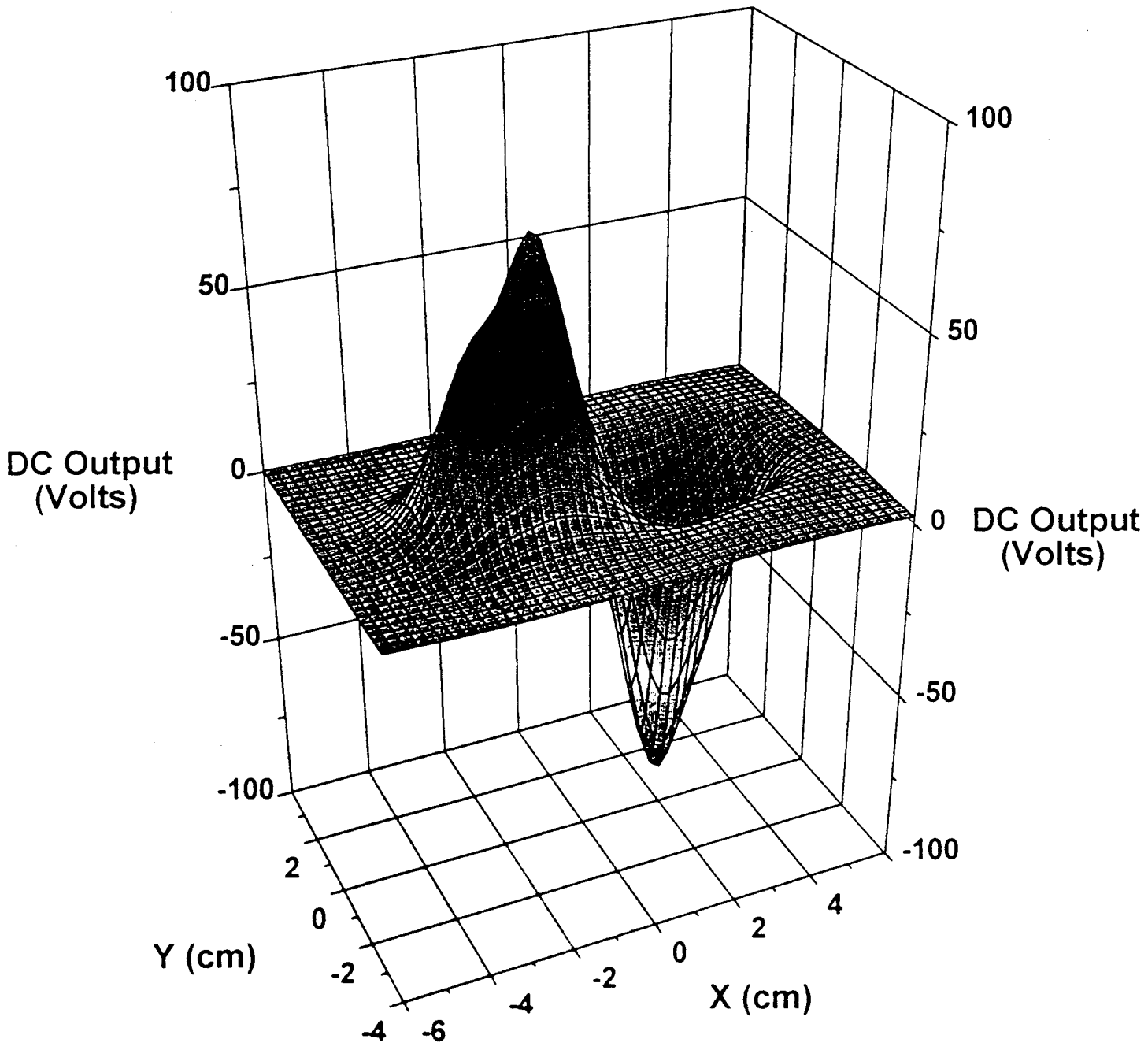

14

Figure 3. Image of 15% strained TRIP steel in the post-magnetized state.

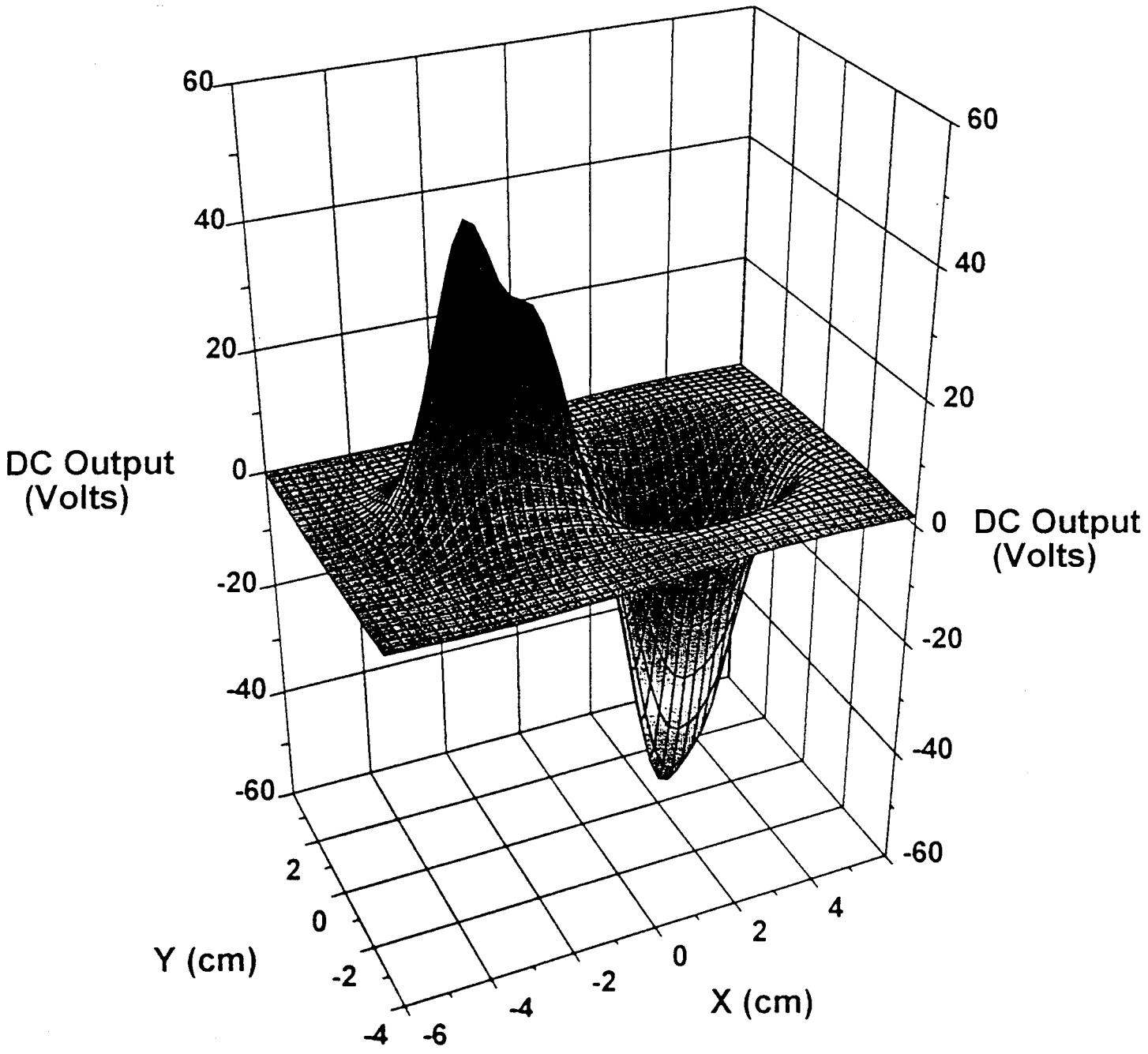

Figure 4. Image of 10% strained TRIP steel in post-magnetized state.

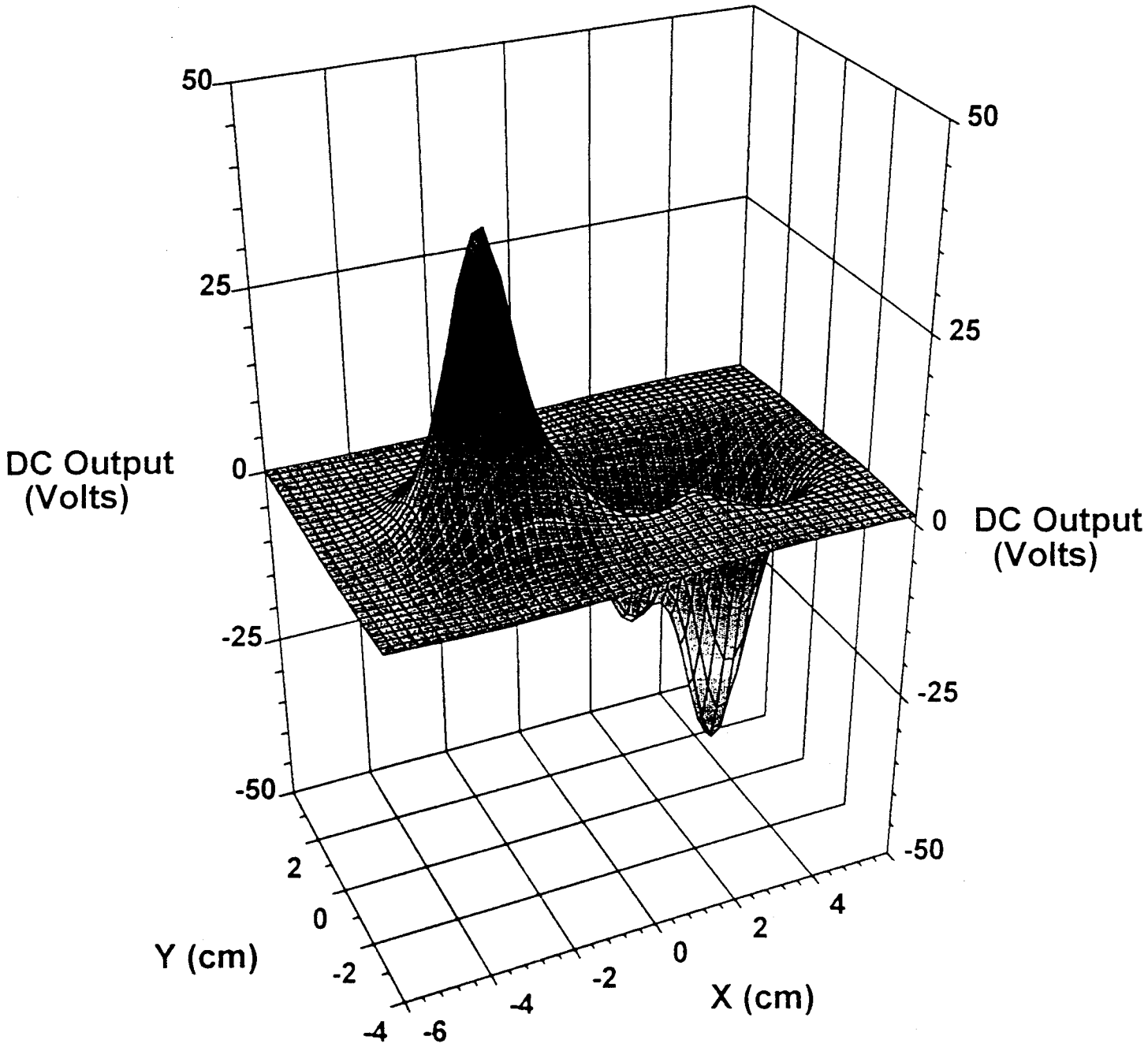

Figure 5. Image of 5% strained TRIP steel in post-magnetized state.

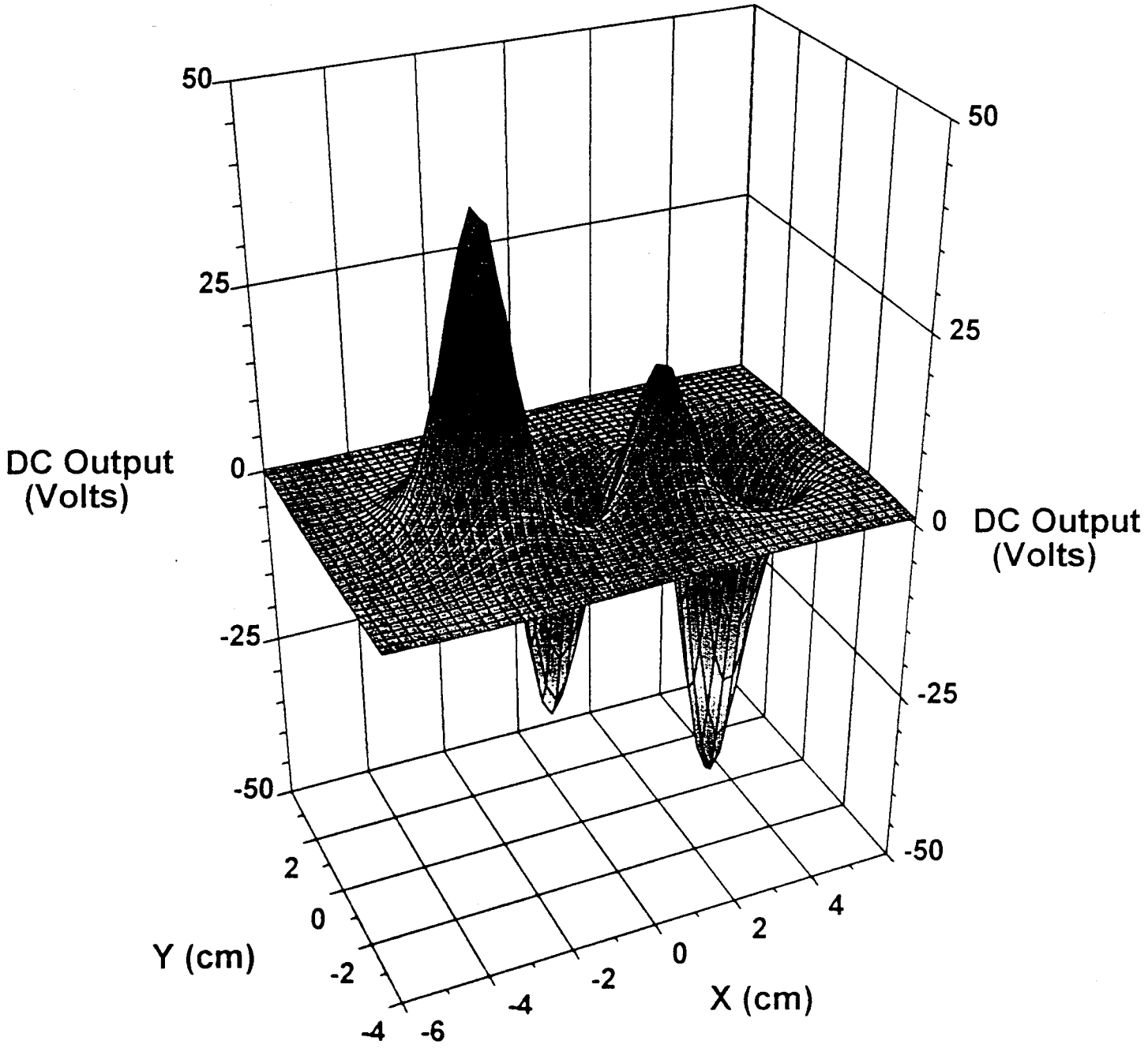

Figure 6. Image of unstrained TRIP steel in post-magnetized state.

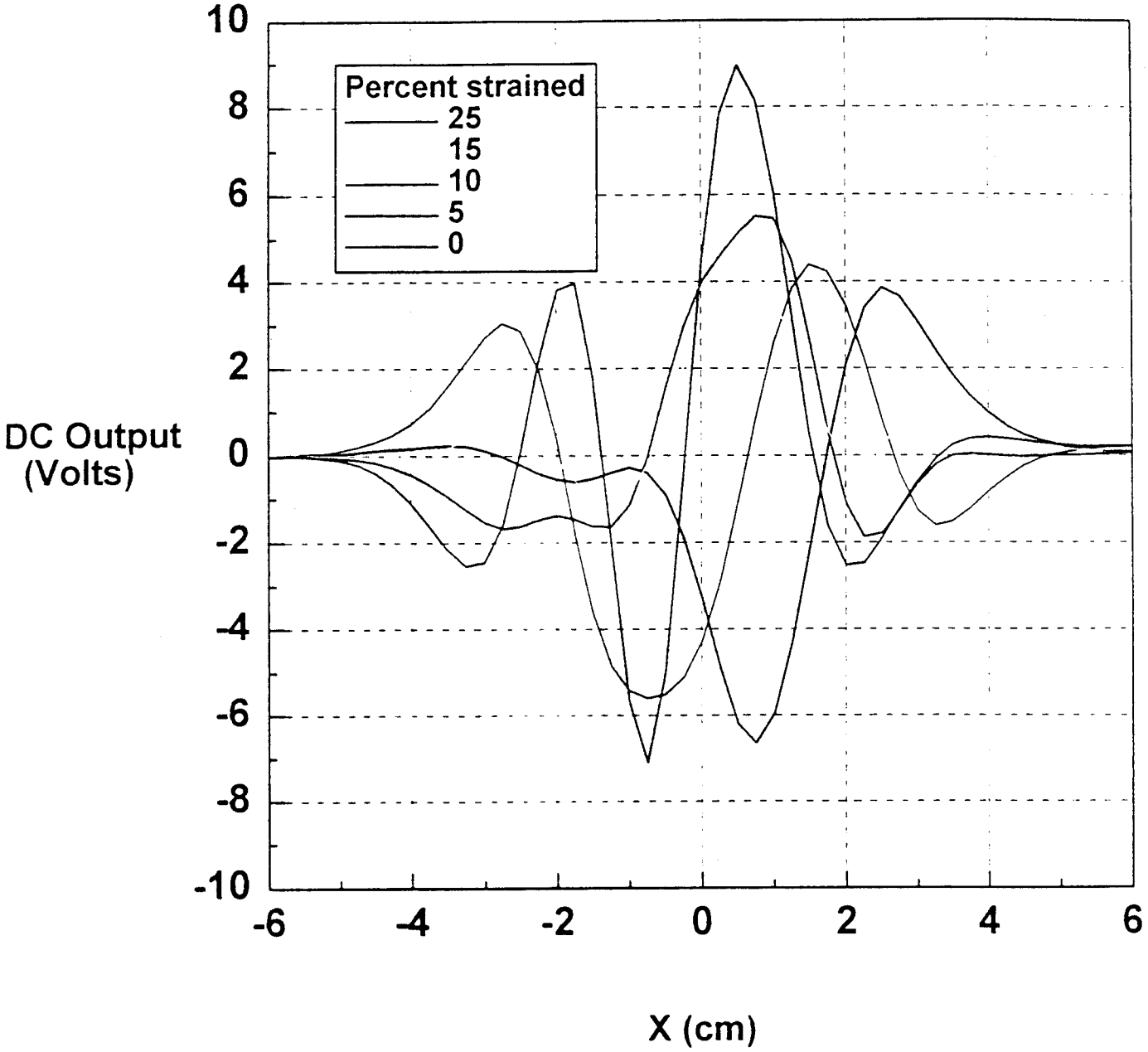

15

Figure 7. Scans along axis of various strained TRIP steel samples. All are in the as-strained unmagnetized state, and show unaligned domain structure along the scan direction, with relatively weak absolute magnitudes.

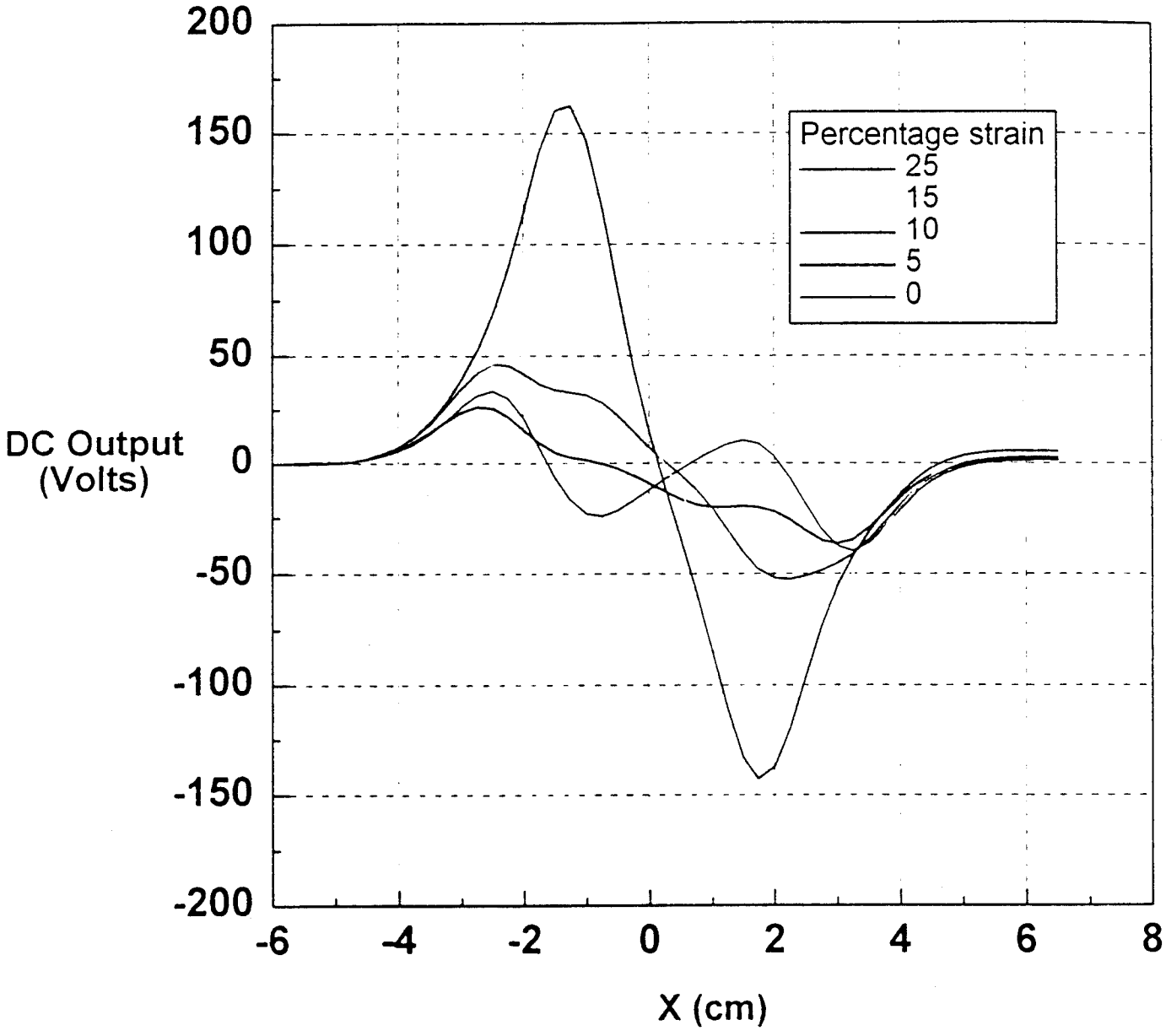

Figure 8. Scans along axis of various strained TRIP steel samples. The samples are in a post-magnetized remanent state. The more strained samples show larger net magnetizations, and tend to have better aligned domains. Larger and more uniform magnetic phases would tend to enhance inter-domain exchange coupling, yeilding both larger moments and stronger shape anisotropy.

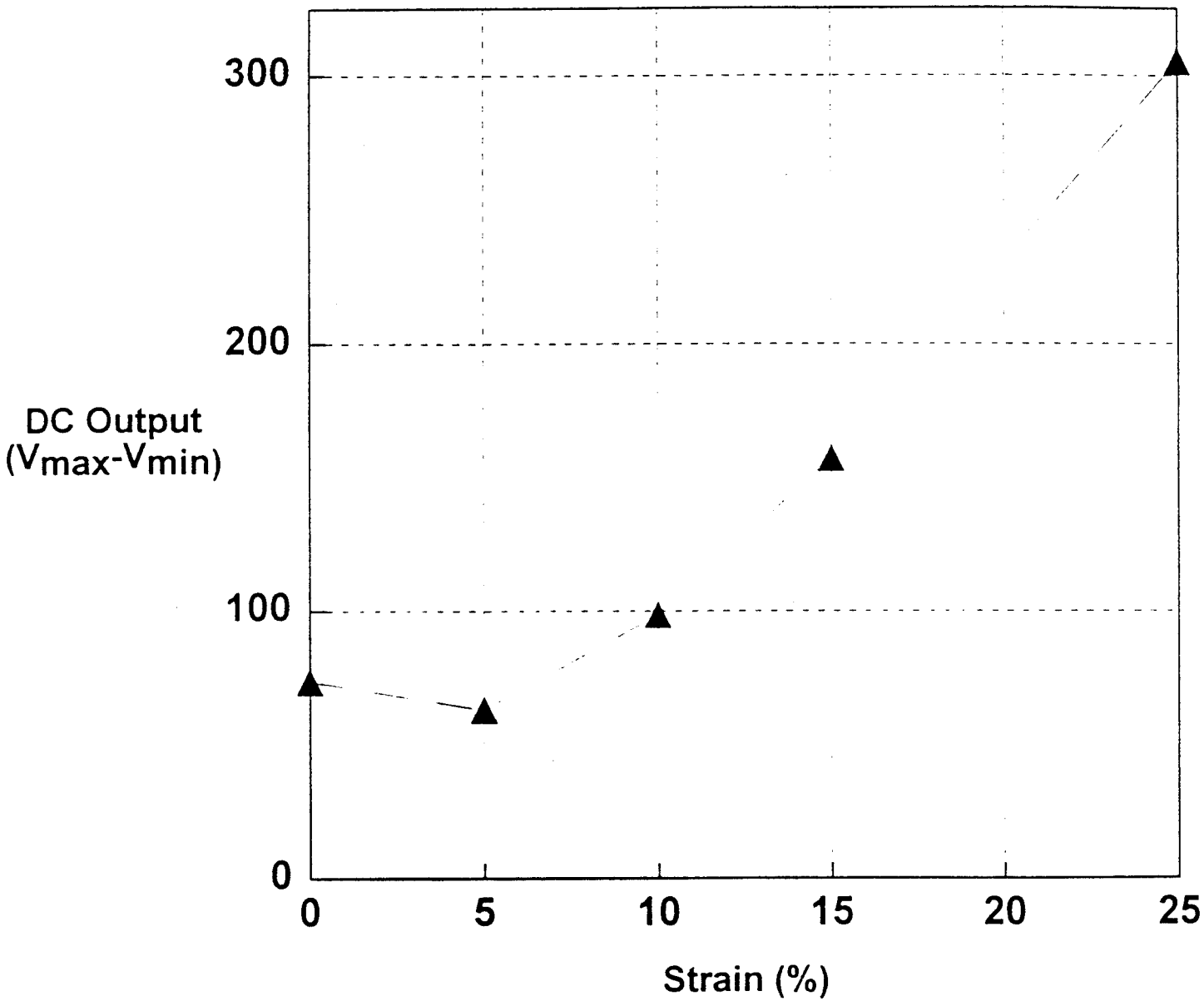

24

Figure 9. The strength of the magnetic signal versus strain is plotted for the TRIP steel samples studied. The signal strength is defined as the maximium voltage swing observed in the scan along the length of a sample in the remanent state following the application of a magnetizing force along the easy axis.

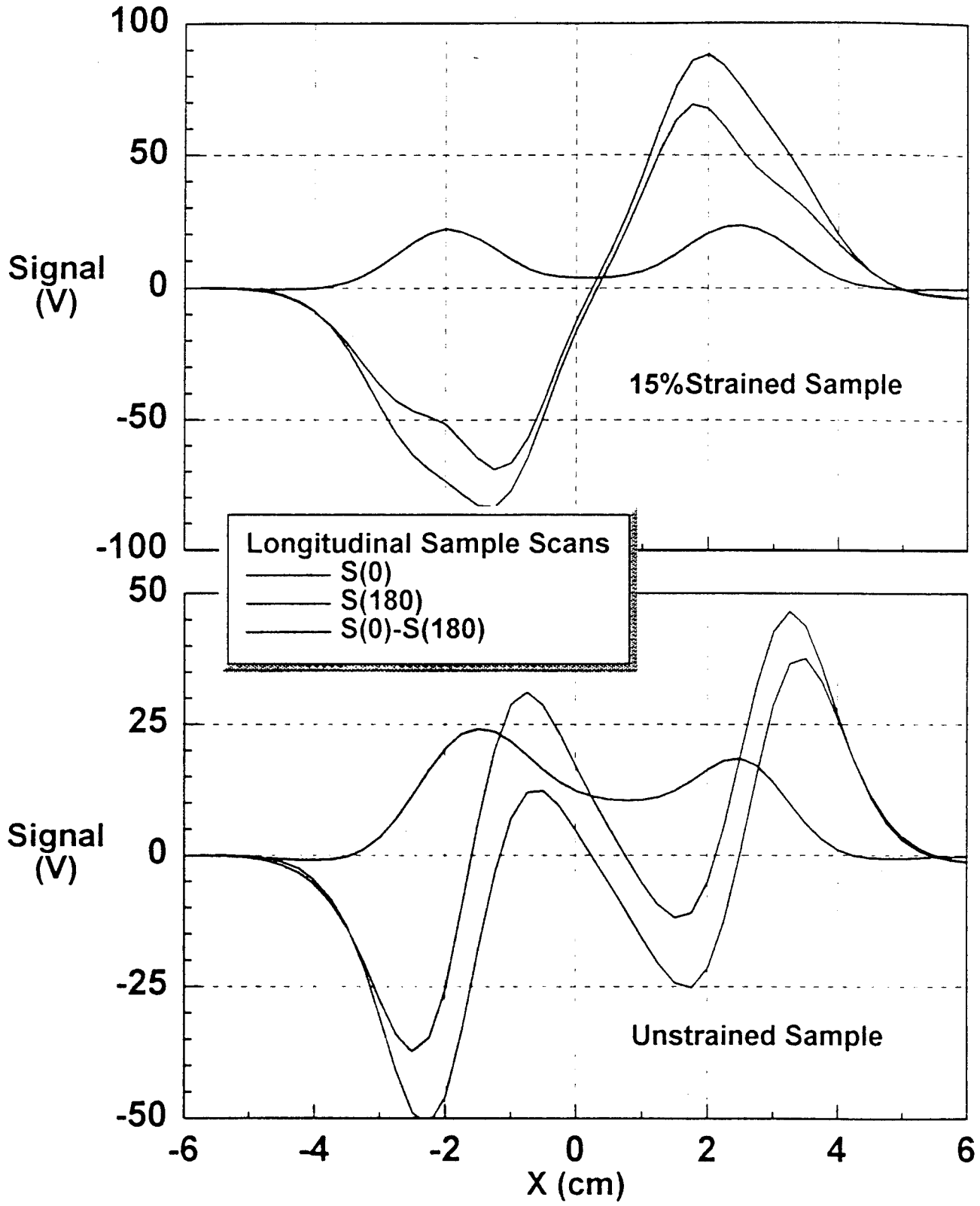

Figure 10. The effect of rotating the TRIP steel samples about the longitudinal (easy) axis is shown for both a strained and unstrained sample. For both samples, a scan is taken in the as-magnetized orientation, and again following a 180 degree rotation. Off-axis magnetizations will be manifested as differences between the scans. (Care must be taken not to also translate the sample.)

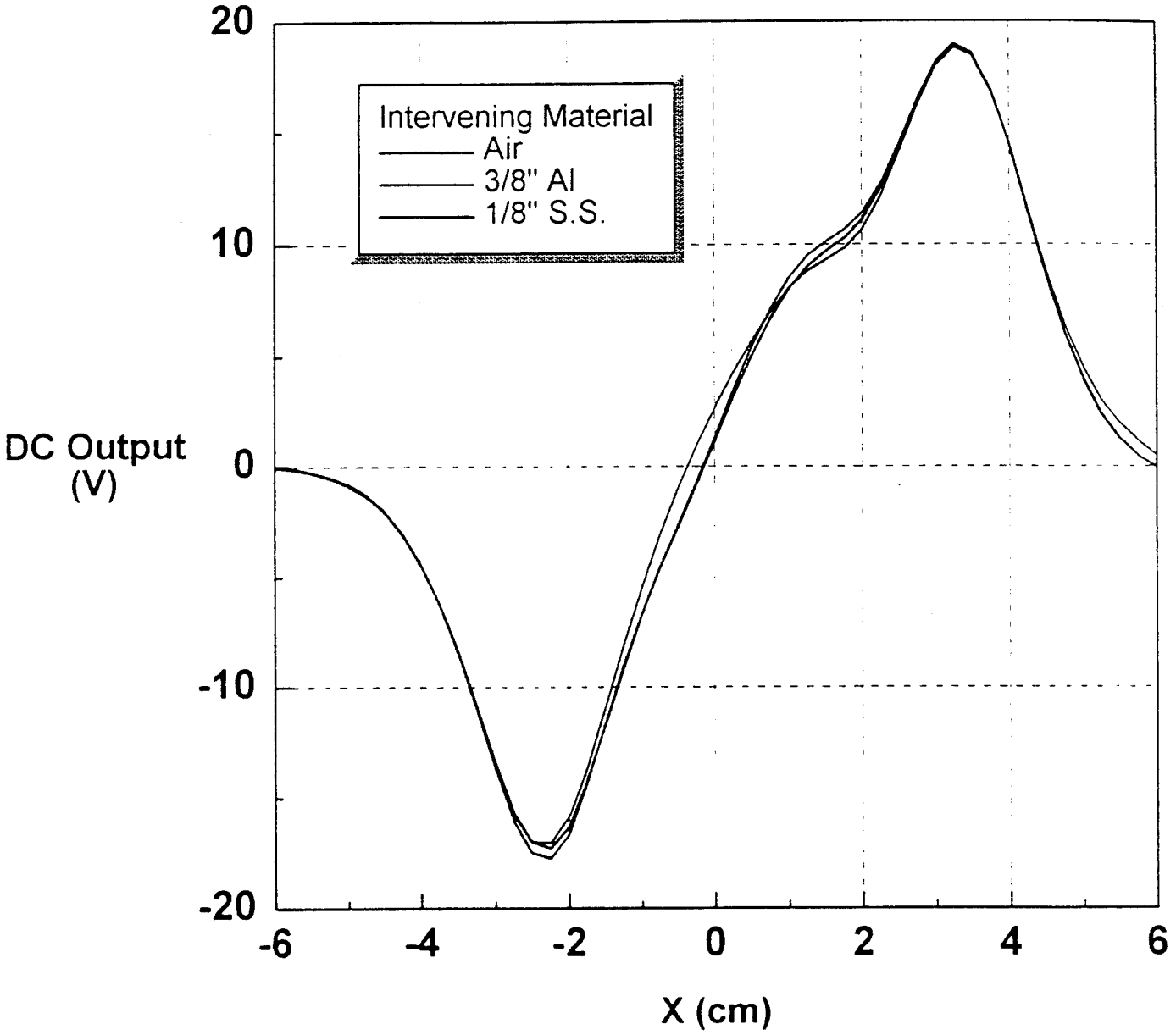

Figure 12. The effect of placing certain intervening materials between the sample and probe tail (1/2" separation for these plots). This demonstrates the remote sensitivity that can be achieved with a magnetic sensor element imbedded within certain structures.

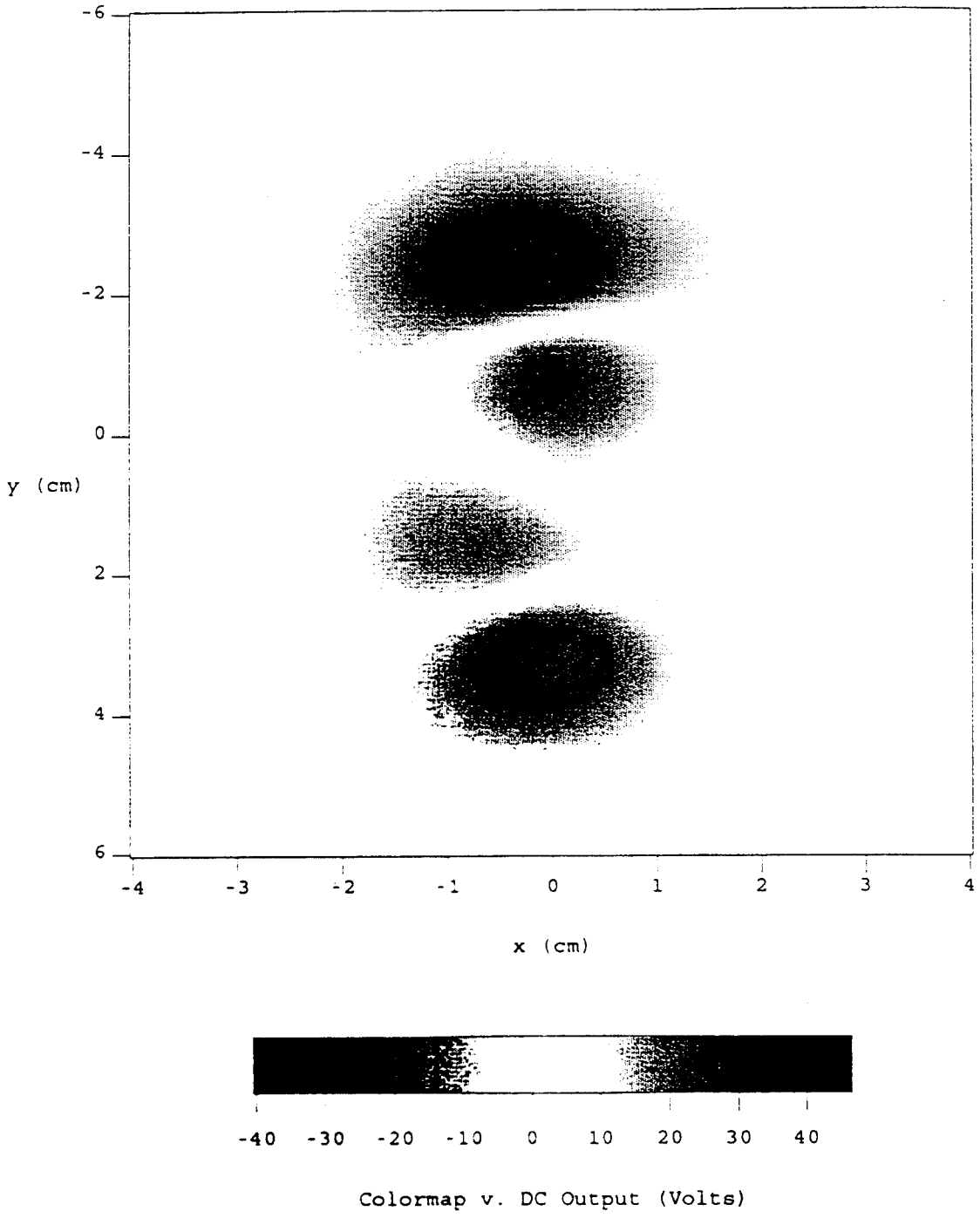

Figure 12. 2-D image of the unstrained magnetized TRIP steel sample showing the transverse component of the magnetization as evidenced by the unaligned negative and positive peaks.

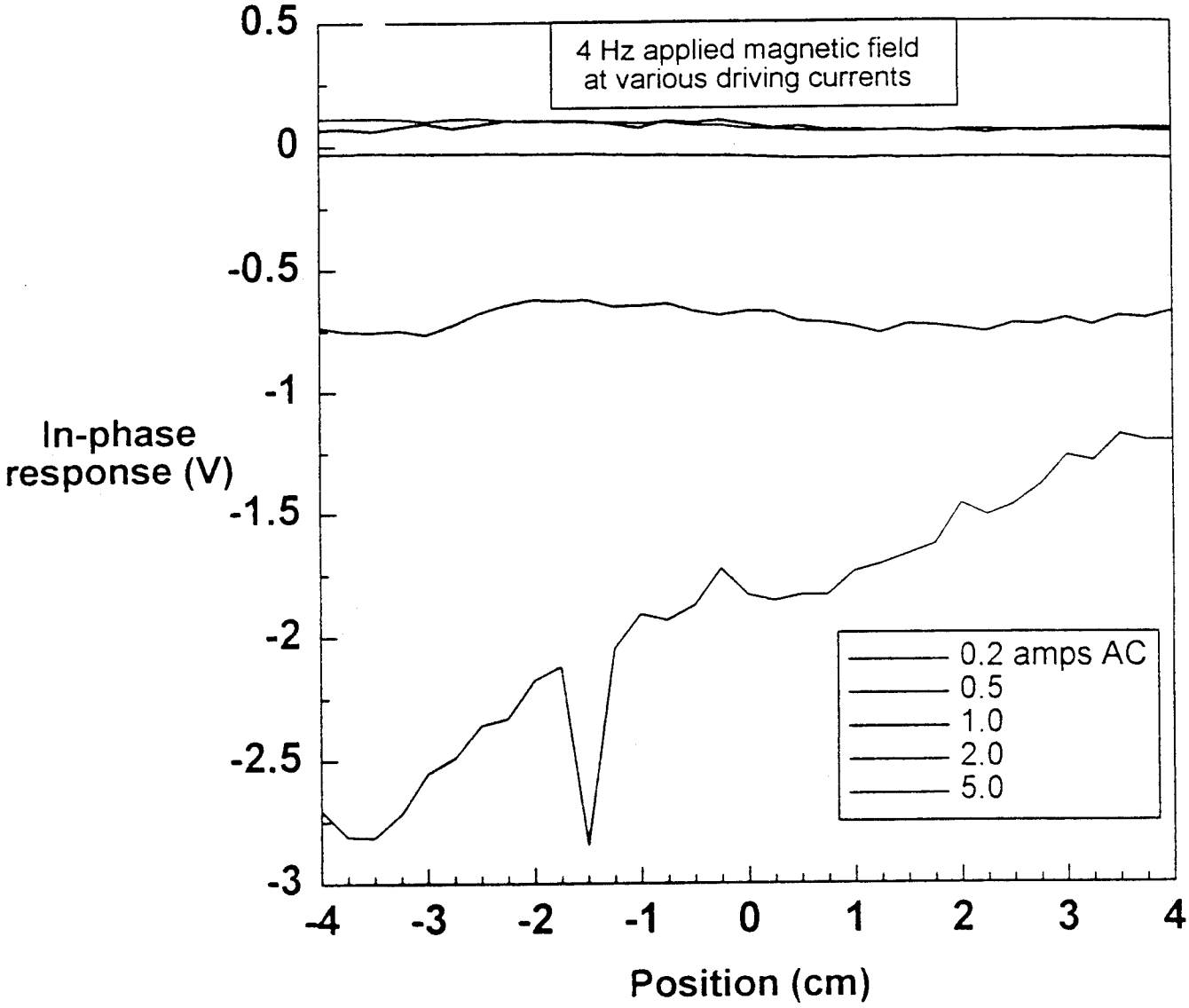

Figure A1. Scans across the edge of Al (approx. the 0 cm position) were taken. The in-phase response for a fixed frequency of 4 Hz for a series of AC magnet driving currents. It is noted that there is little in-phase response, although the noise and drift can be seen to increase with driving current.

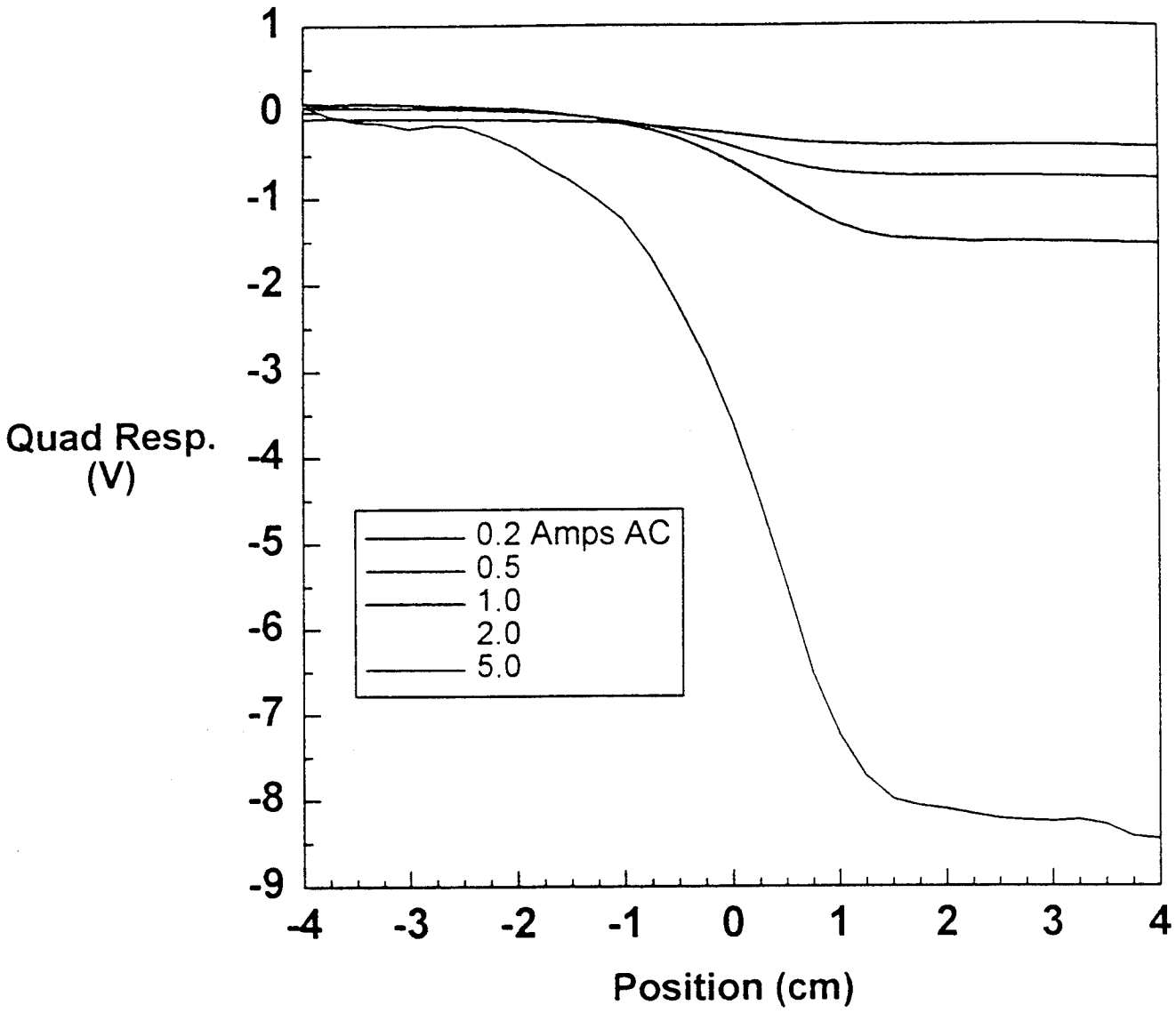

Figure A2. The quadrature response from a series of scans across the edge of a 3/8" Al plate (edge at 0 cm position) is shown. A 4 Hz current is driving the magnet at the labeled current amplitudes. For this arrangement, we obtain a linear response with magnetic field, here 1.6 V/A.

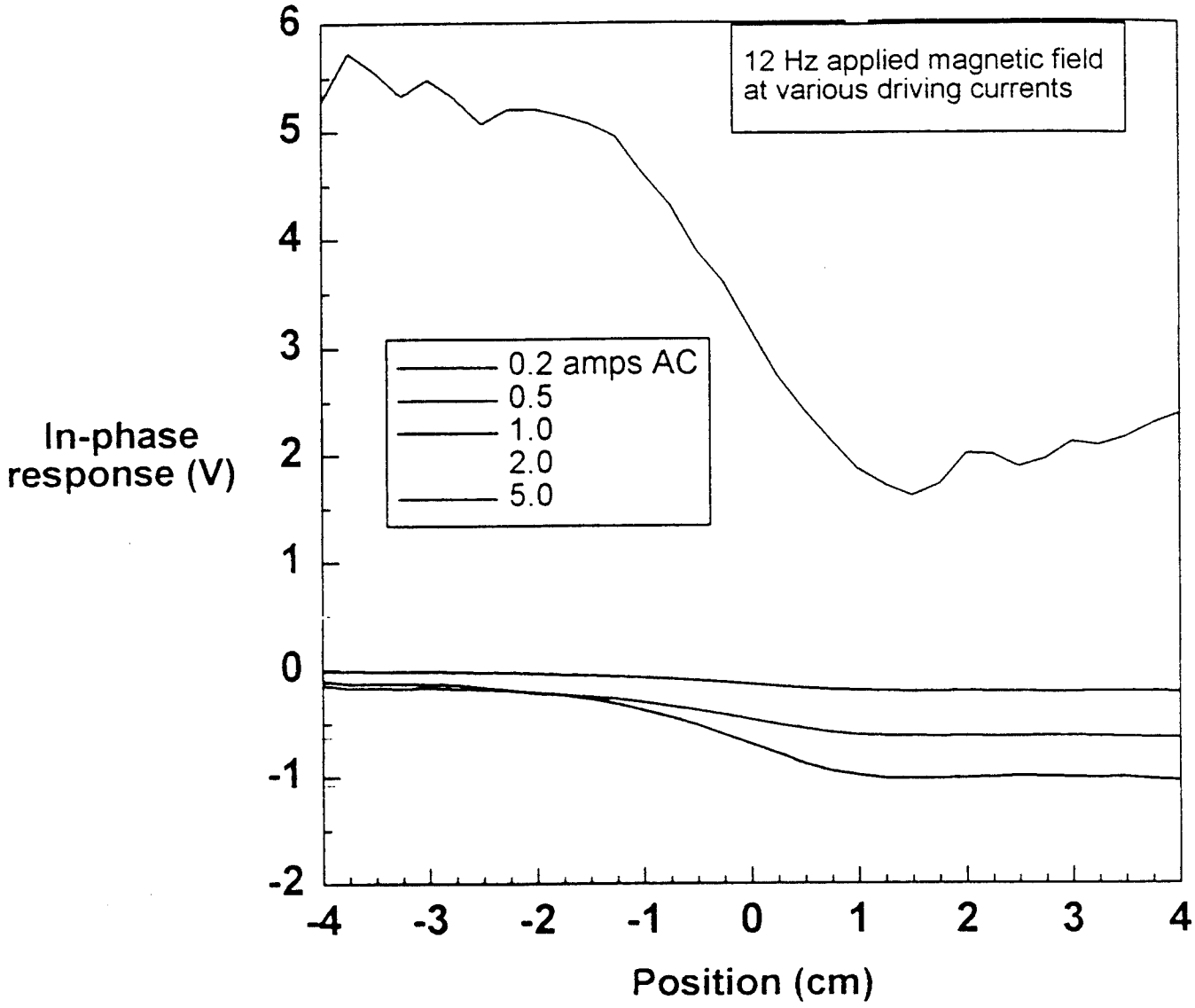

Figure A-3. The in-phase response of scans across the edge of an Al plate (at 0 cm). The magnet is driven at 12 Hz and at the indicated current. While the amplitude of the response scales approximately linearly with current, there is a notable increase in noise and drift above 1 amp.

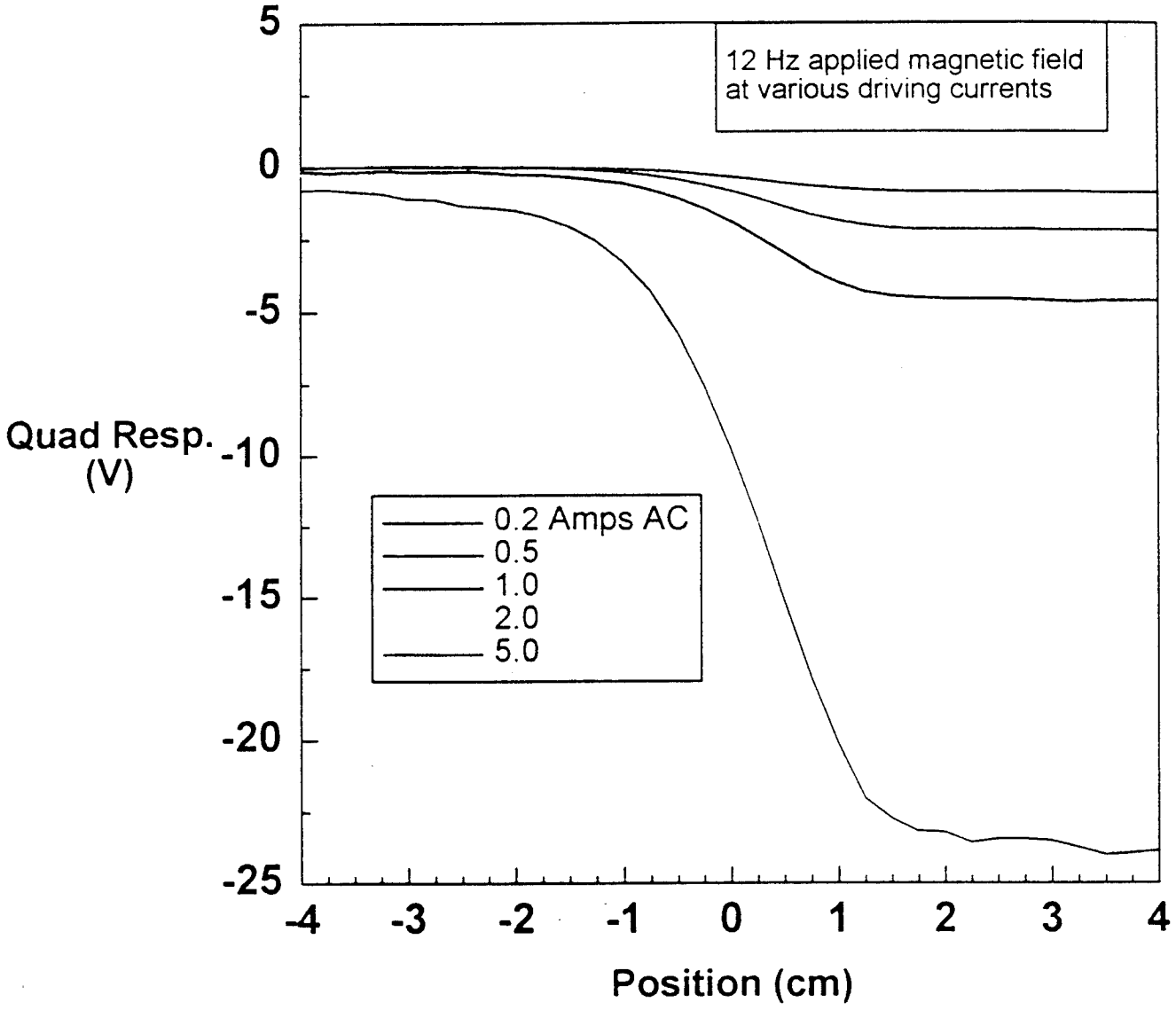

Figure A4. The quad response for a series of scans across the Al plate edge at 12 Hz and various currents as indicated. The response is linear with current, with a constant of proportionality of 4.5 V/A.

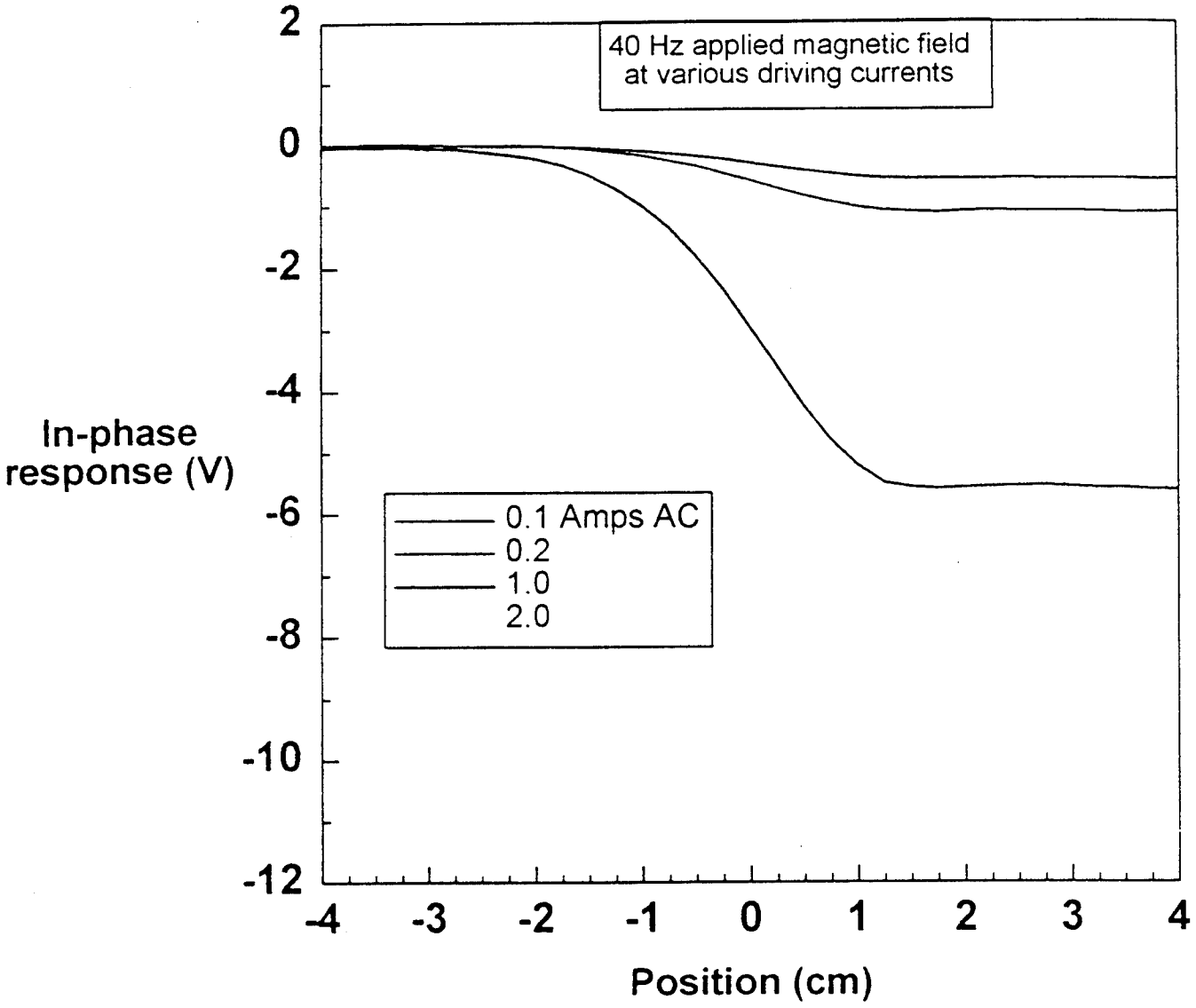

Figure A5. Another series of scans across the Al plate edge reveal that the in-phase response at 40 Hz is distinct at all magnet currents. There is a significant rotation of the system response at this frequency.

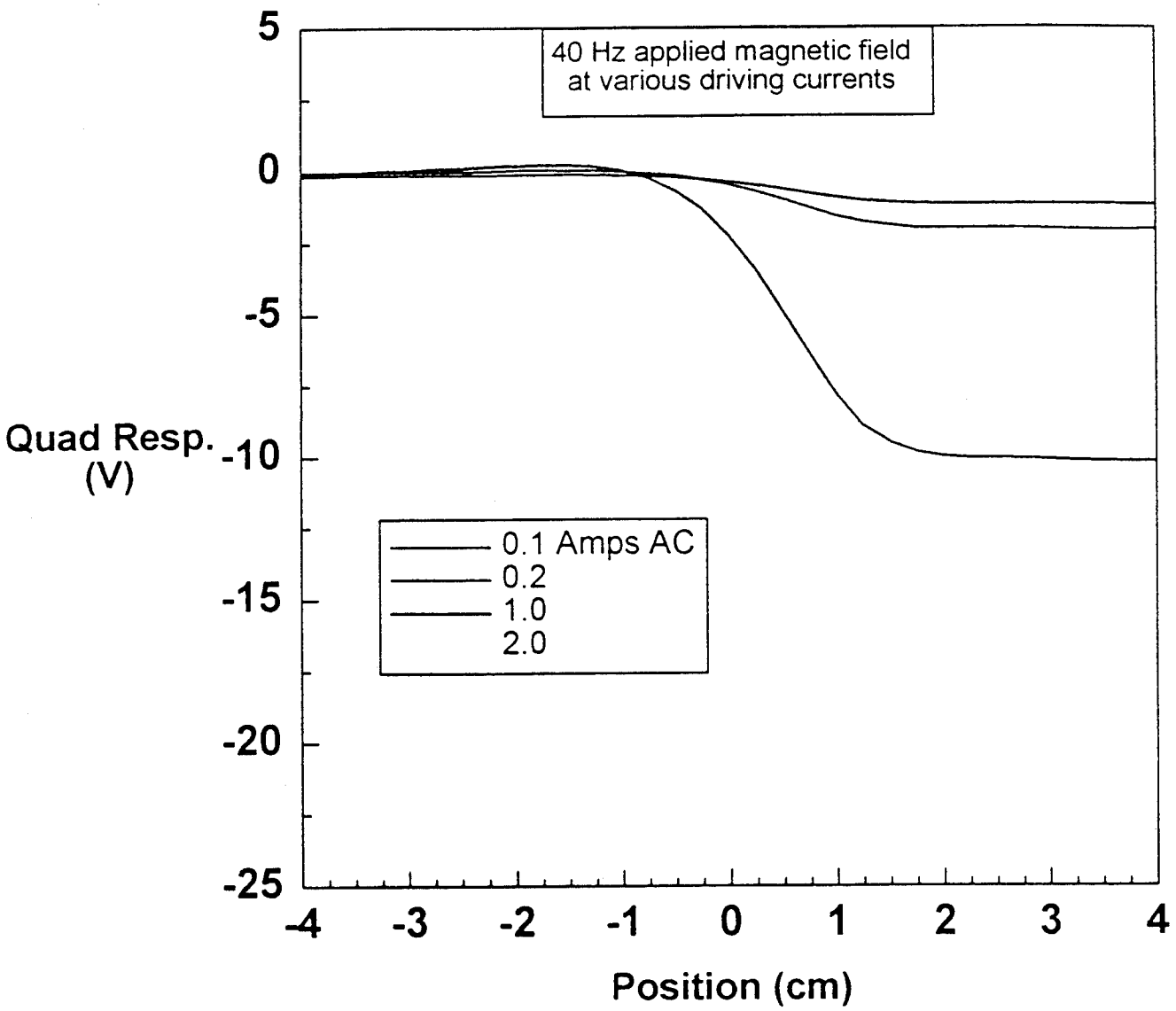

Figure A6. The quad response from a series of scans at varying magnet currents across the edge of an Al plate. The AC frequency is 40 Hz. The response is again proportional to the magnet current, and the constant of proportionality is 10.1 V/A.

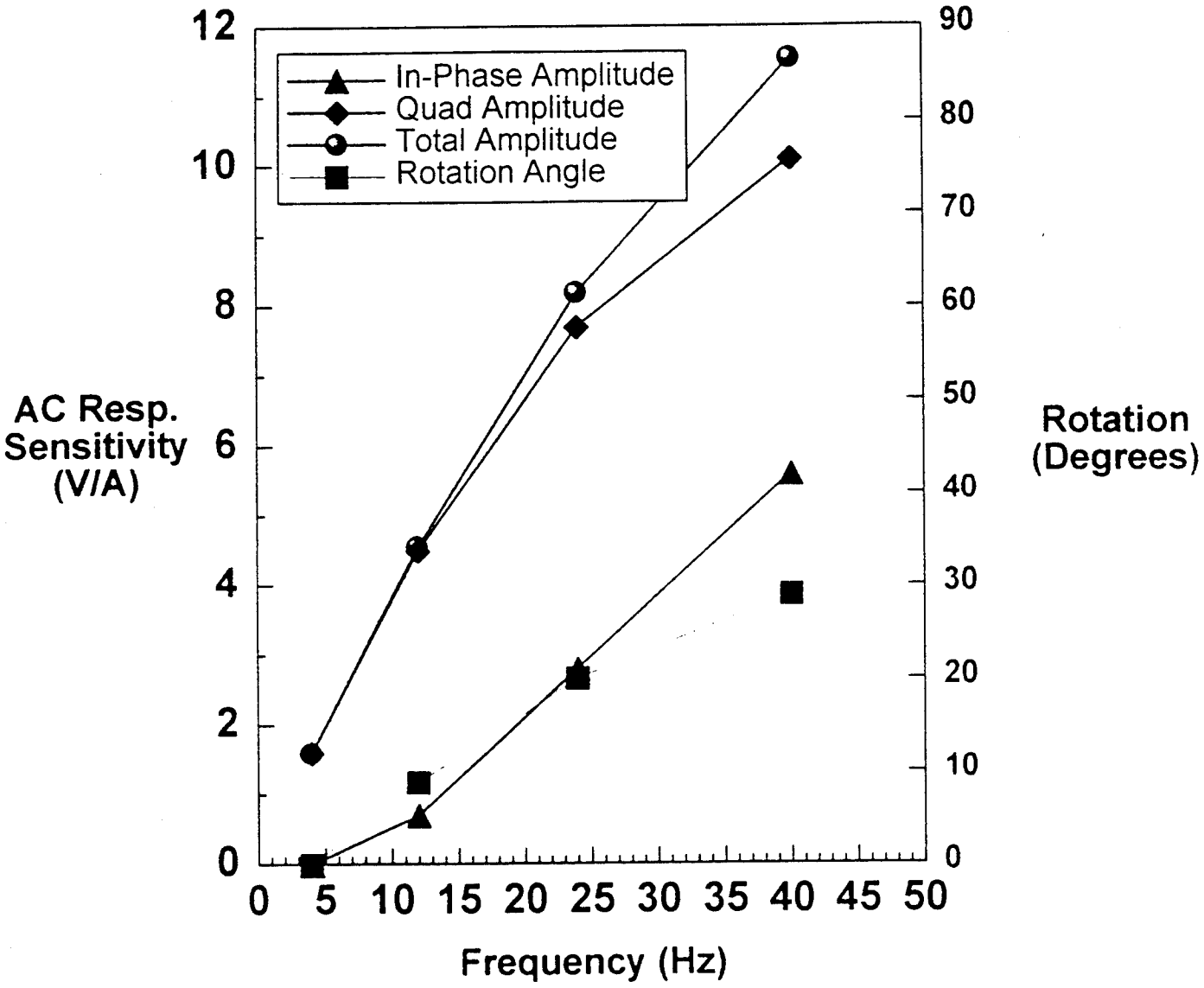

Figure A7. Shown are the sensitivities of the in-phase, quad and total responses in units of volts/amp driving current. It is seen that the in-phase response increases above 10 Hz, with a corresponding roll-off of the quad sensitivity. Overall, the sensitivity increases less than proportionally with frequency above about 20 Hz. Also shown is the relative angular rotation of the system response as a function of frequency.

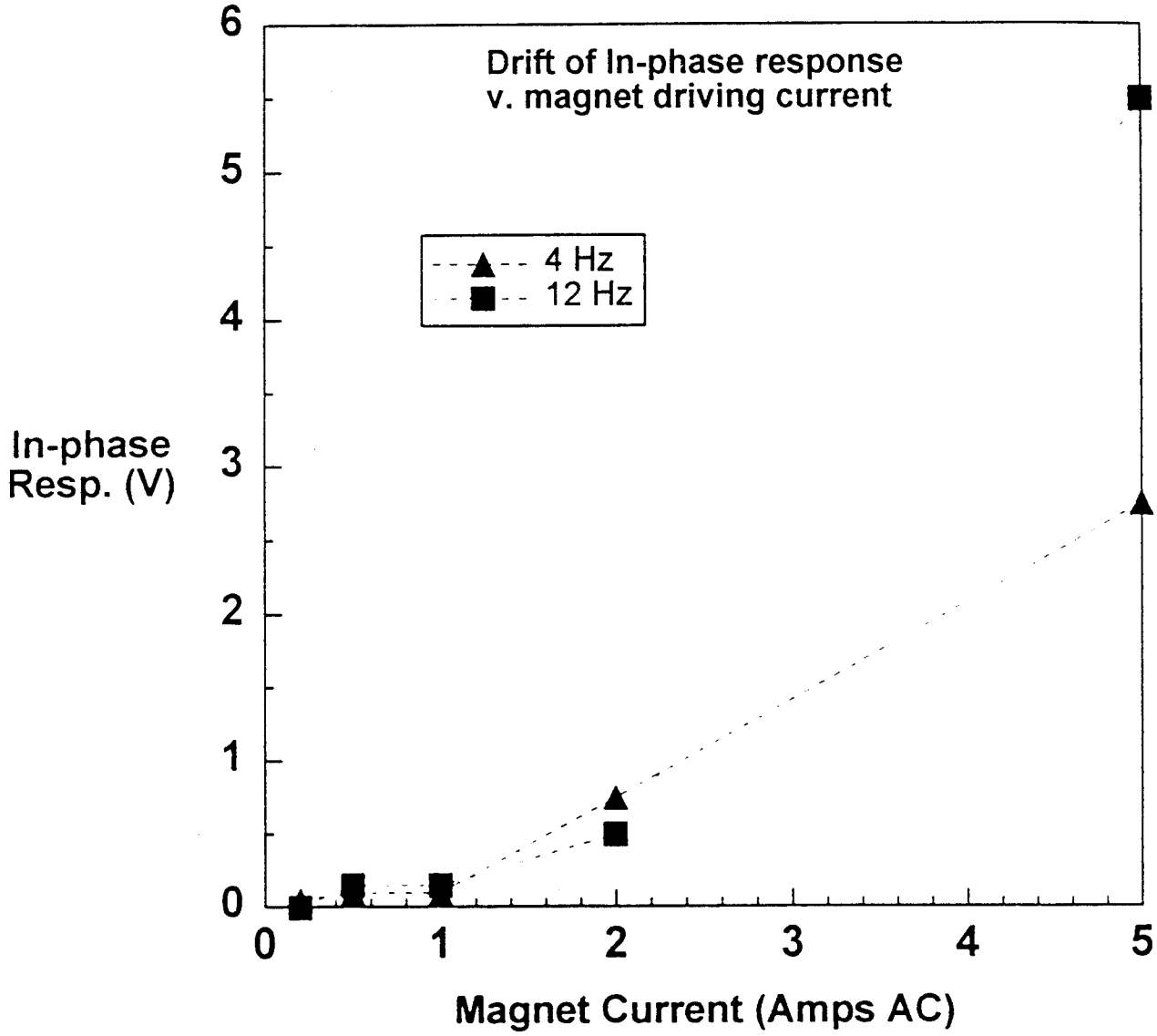

Figure 21. The observed drift that occurred between nulling the system response through the MDAC settings and taking the ensuing data scan. These data illustrate the impact of the higher current settings on the system stability, but do not quantitatively characterize the relationship.

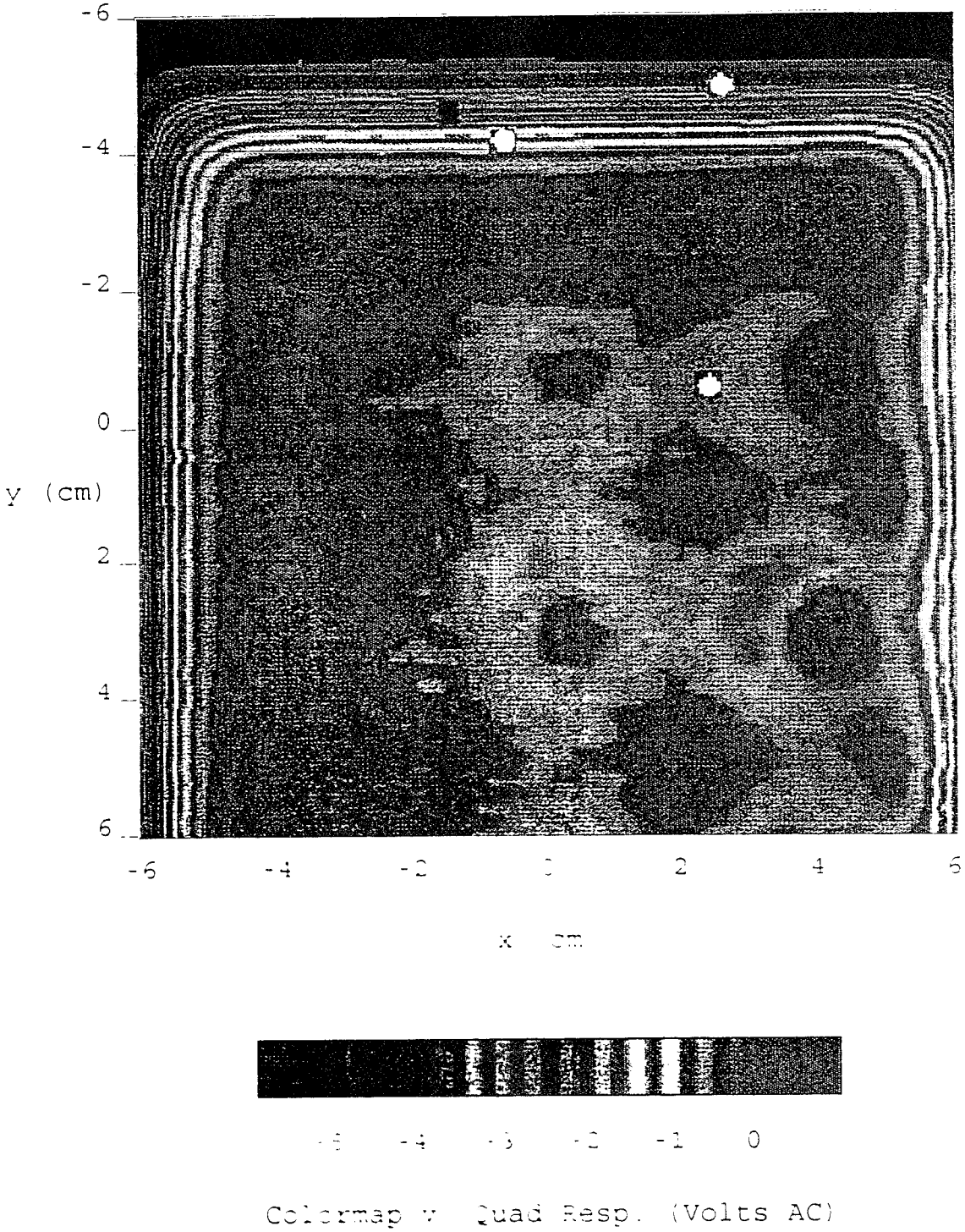

Figure A9. Image of 3/8" Al plate generated by the quad response of 24 Hz magnetic field with driving current of 1 amp. The plate has various holes as described in the text. The edges of the Al plate are at (y = -6 cm), and (x = +7.3, -7.1 cm). It is seen that the relatively remote straight edges contribute significantly stronger signals than the holes.

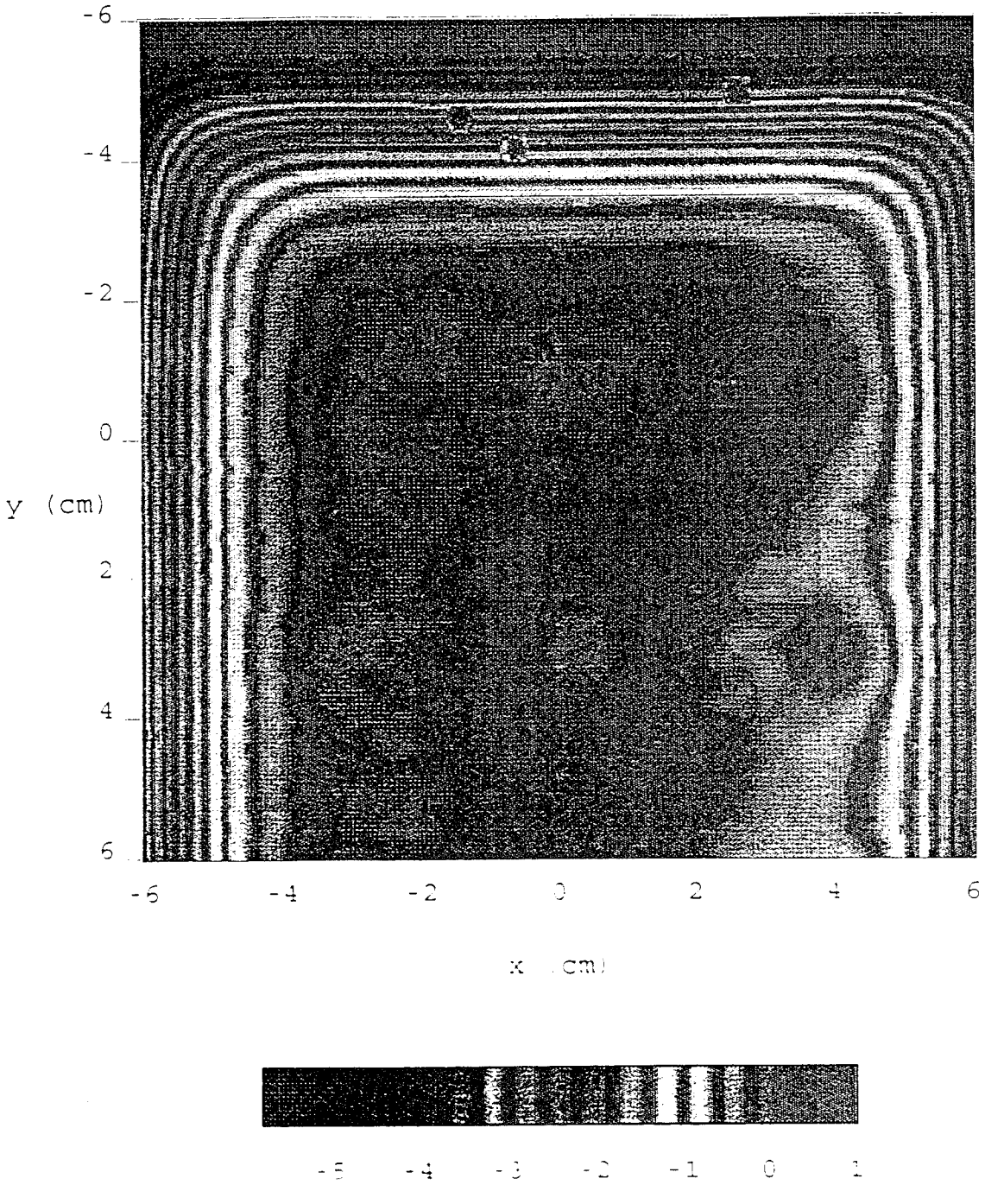

Figure A10. Image of 3/8" Al plate generated by the in-phase response of 24 Hz magnetic field with driving current of 1 amp. The plate has various holes as described in the text. The edges of the Al plate are at (y = -6 cm), and (x = +7.3, -7.1 cm). It is seen that the relatively remote straight edges contribute significantly stronger signals than the holes

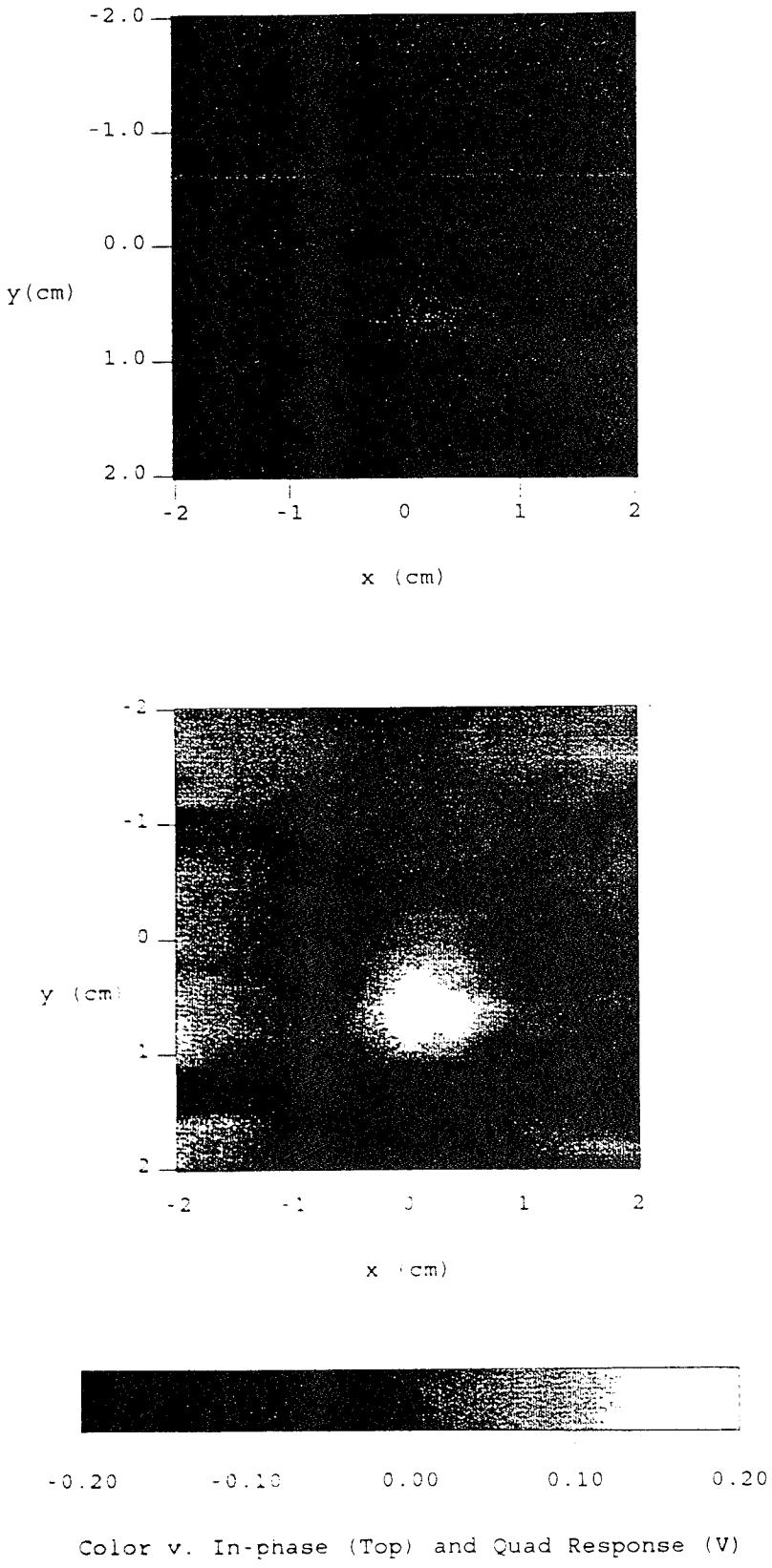

Figure A11. In-phase and quad images of center hole of array.

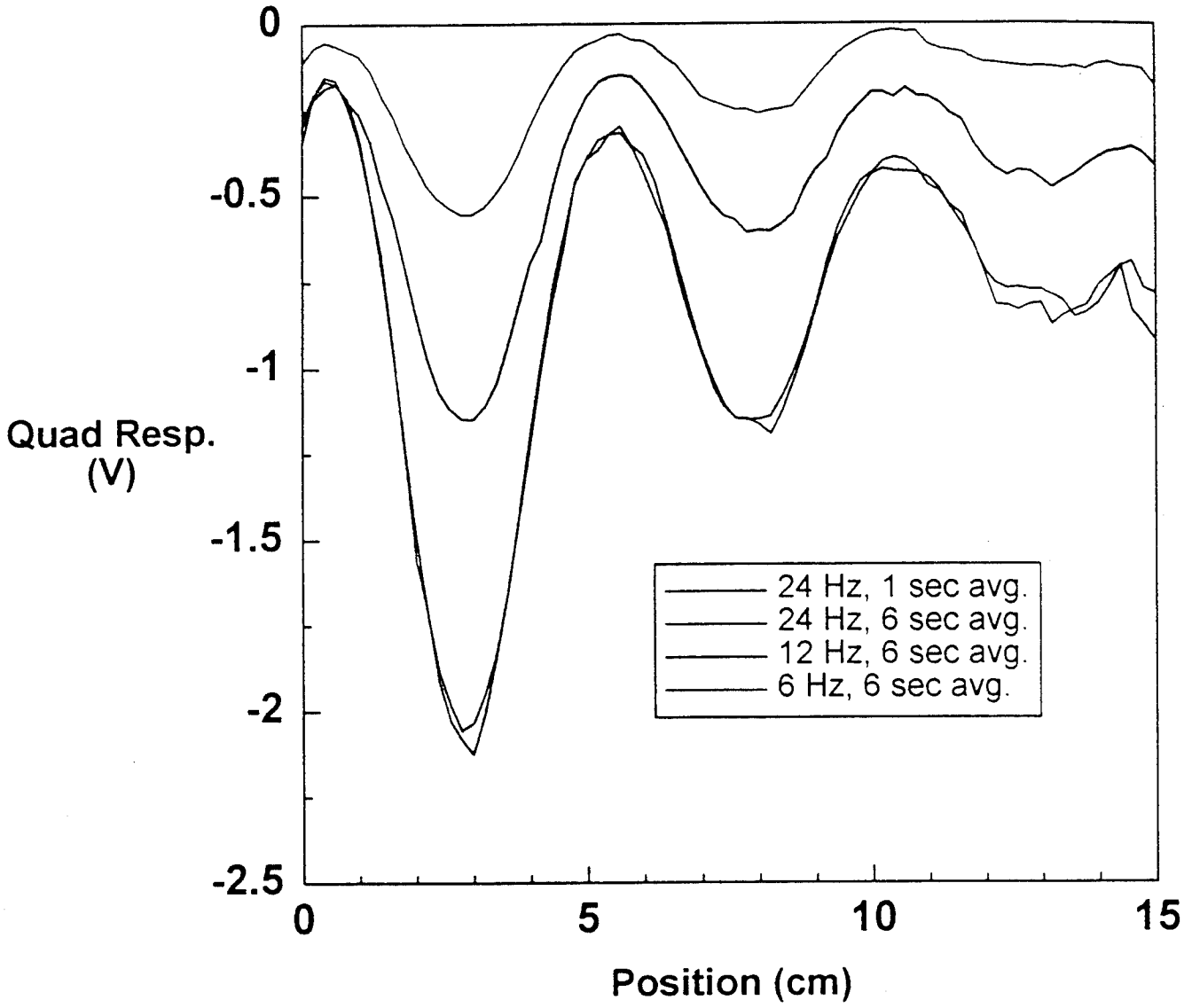

35

Figure G1. Scans across a 1/2" Al plate with three grooves of depths 1/4", 1/8", and 1/16" cut in top surface. The legend indicates the experimental differences among the scans.

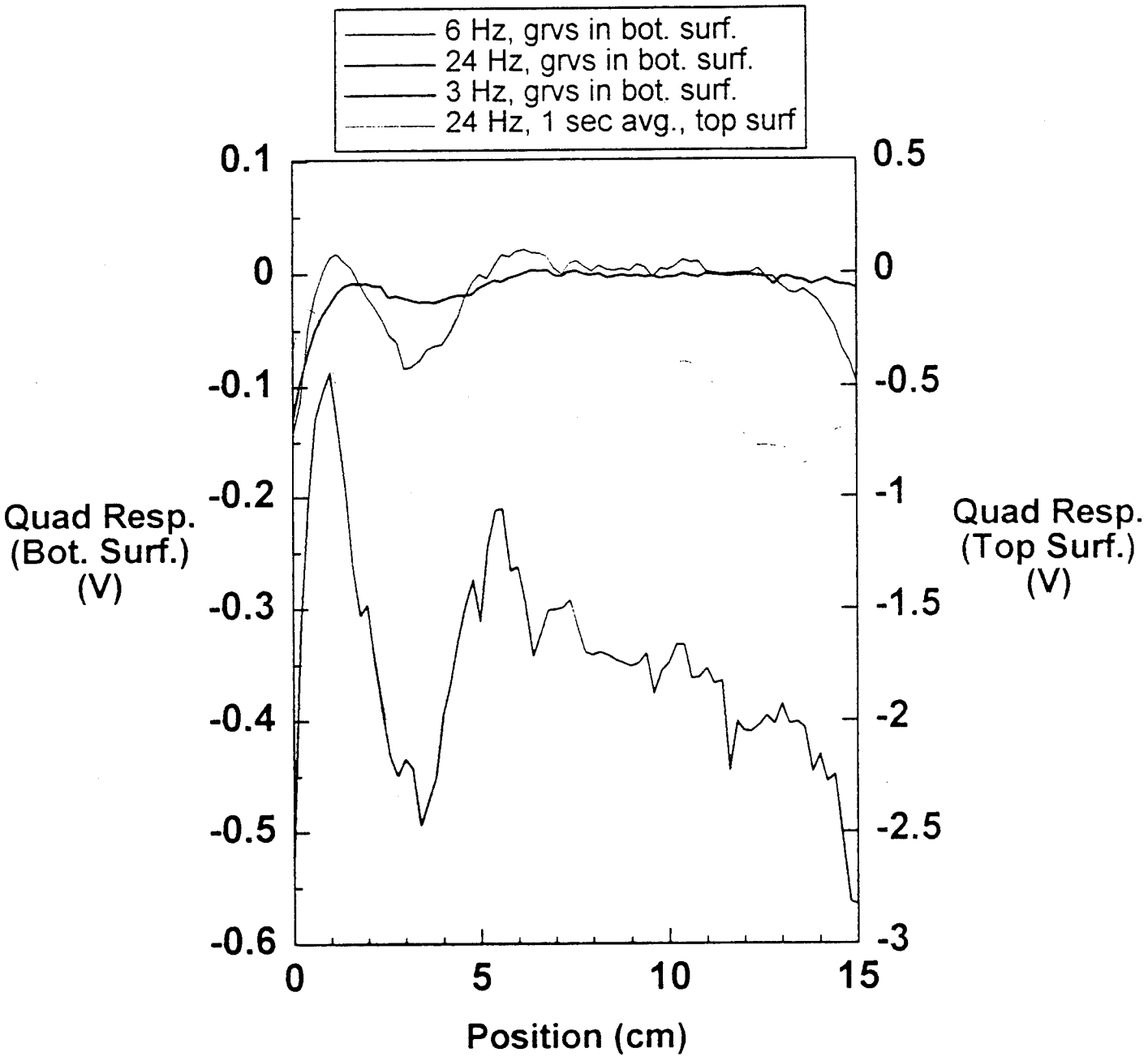

Figure G2. Scans across the same grooves, but with the grooves on the bottom surface of the 1/2" Al plate. Only the 1/4" deep groove is apparent. The increased distance from the tail is probably largely responsible. A scan of the same grooves on the top surface (on a separate scale) is included for comparison.

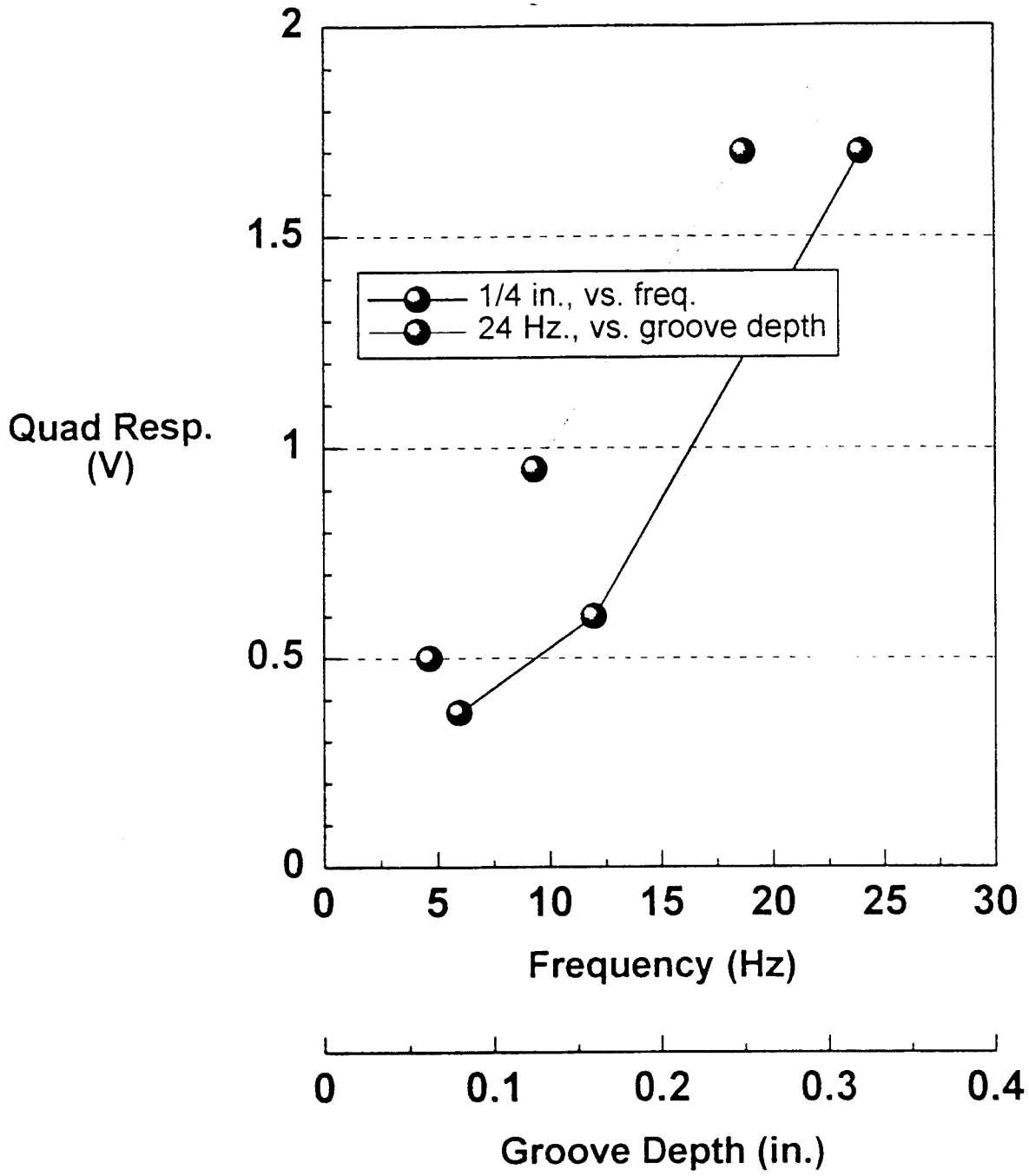

7

Figure G3. The response as a function of groove depth and driving frequency is shown.

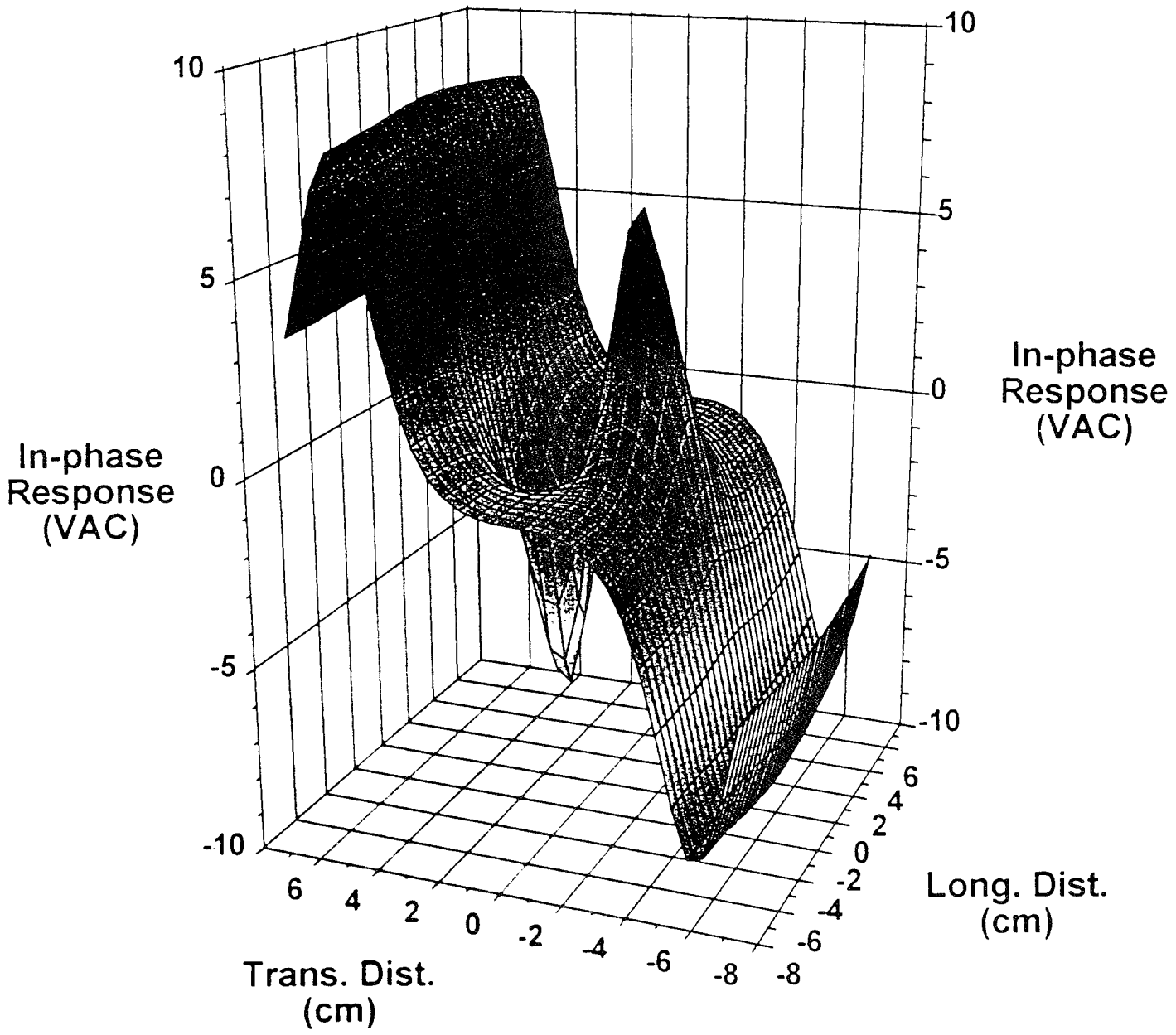

Figure 2-1. Magnetic image generated by in-phase response due to a 1 Amp, 12 Hz AC current passing through the length of an Al plate 4" wide, 1/4" thick with a slot cut in the direction transverse to the current. The slot is 1" long, 1/8" wide, and is centered within the width of the plate. In the above plot, the slot is located at the origin.

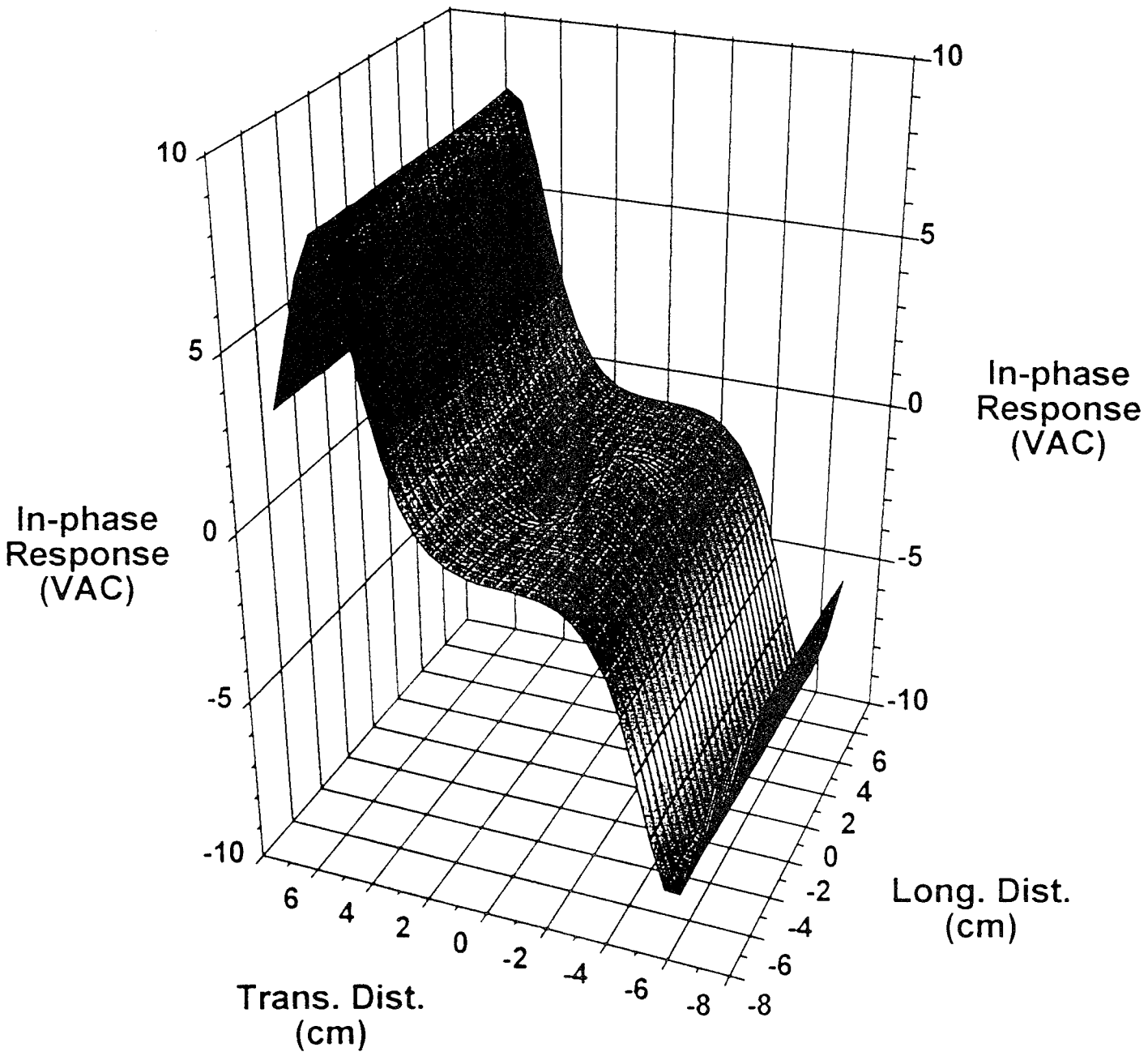

Figure ~~2-1~~. Magnetic image generated by in-phase response due to a 1 Amp, 12 Hz AC current passing through the length of an Al plate 4" wide, 1/4" thick with a slot cut in the direction parallel to the current. The slot is 1" long, 1/8" wide, and is centered within the width of the plate. In the above plot, the slot is located at the origin.

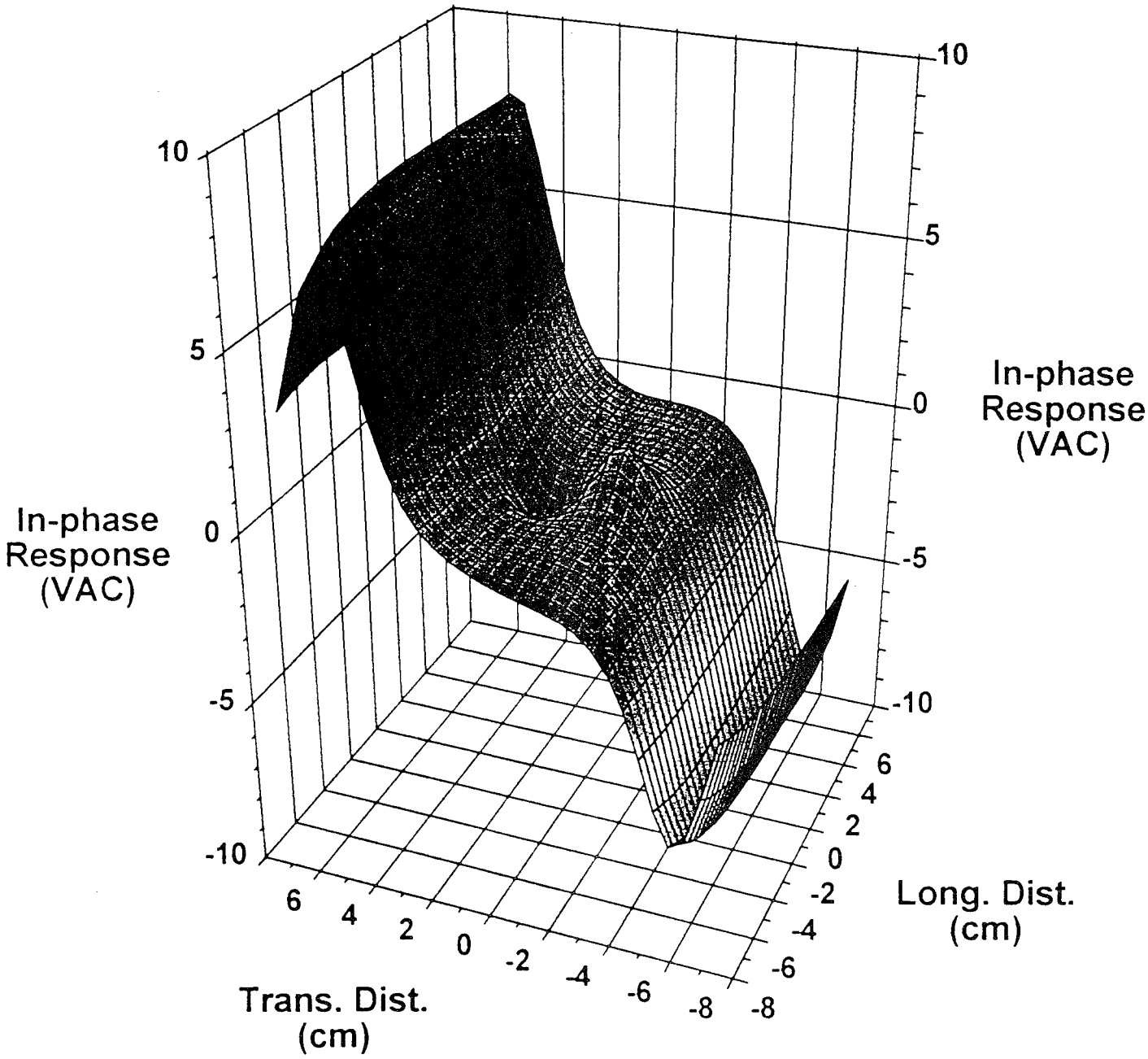

Figure 2-3. Magnetic image generated by in-phase response due to a 1 Amp, 12 Hz AC current passing through the length of an Al plate 4" wide, 1/4" thick with a slot cut in the direction transverse to the current. The slot is 1" long, 1/8" wide, and 1/8" deep into the topside, and is centered within the width of the plate. In the above plot, the slot is located at the origin.

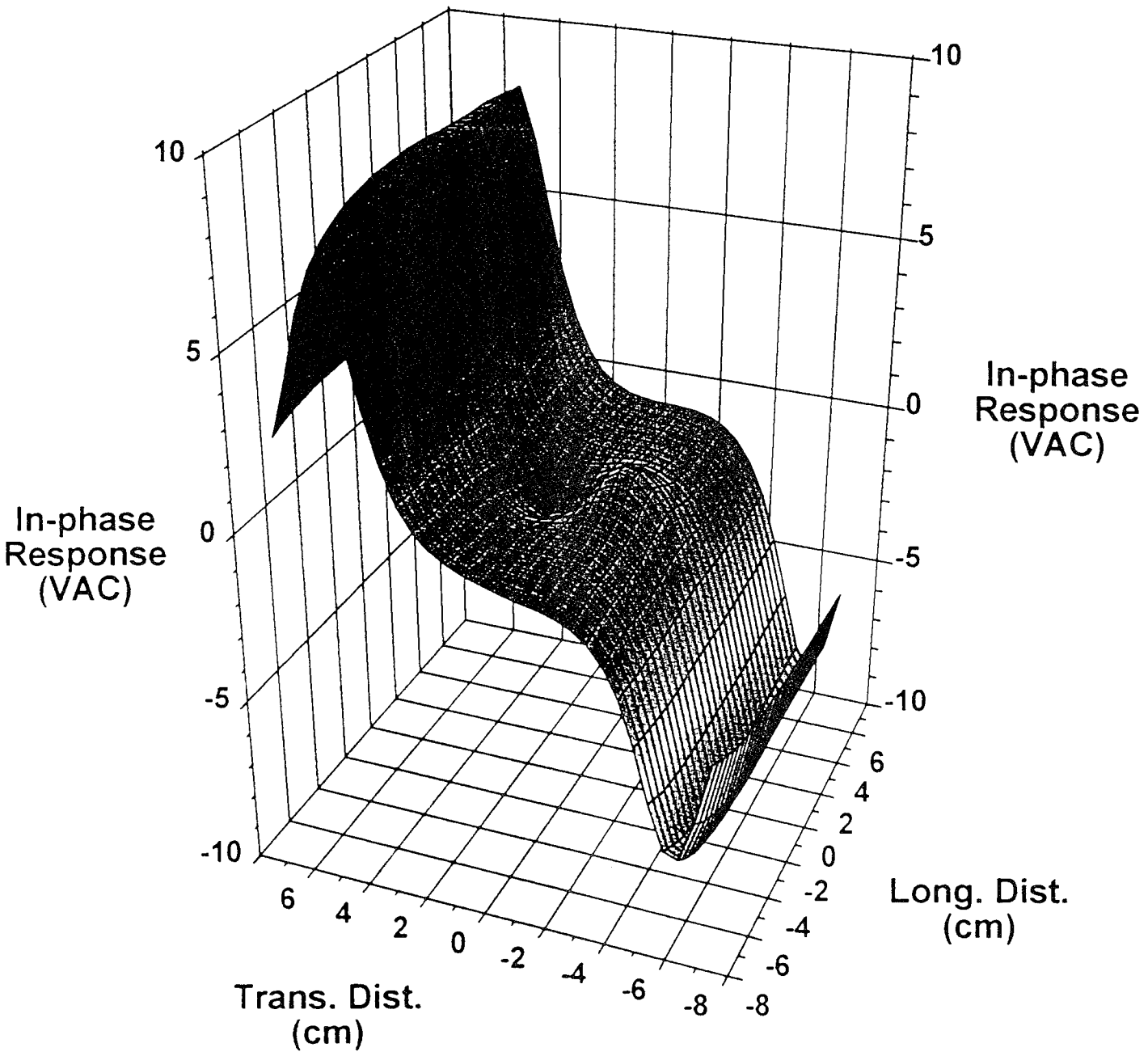

Figure ~~2-4~~ 41. Magnetic image generated by in-phase response due to a 1 Amp, 12 Hz AC current passing through the length of an Al plate 4" wide, 1/4" thick with a slot cut in the direction transverse to the current. The slot is 1" long, 1/8" wide, and 1/8" deep into the bottomside, and is centered within the width of the plate. In the above plot, the slot is located at the origin.

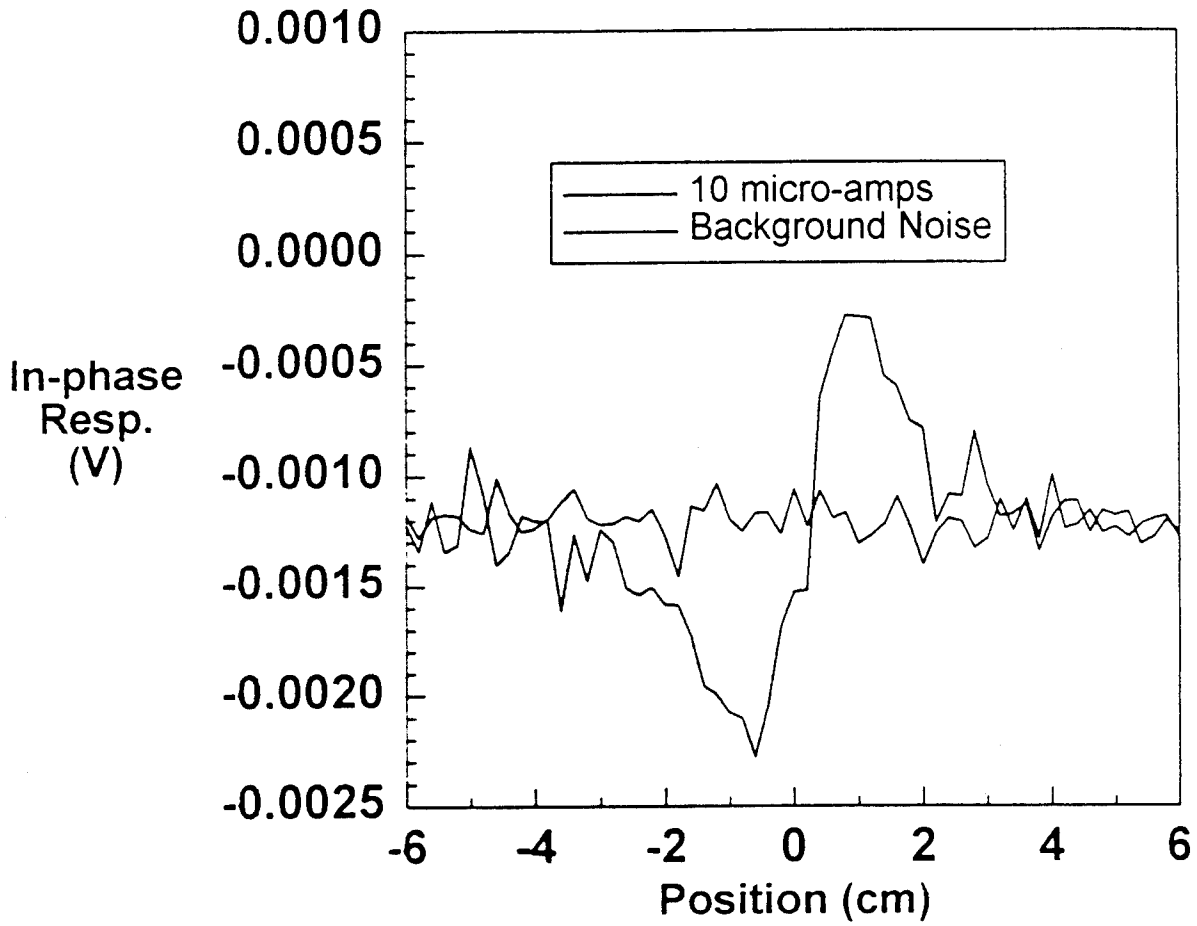

Figure 42. Scan across 0.003" Cu wire carrying 10 micro-amps (AC) current. Also shown is a representative trace of the background noise. The averaging time is 1 second per position, with a stepsize for these scans of 2 mm. The AC frequency is 12 Hz. Indications here are that the sensitivity is 1 micro-amp

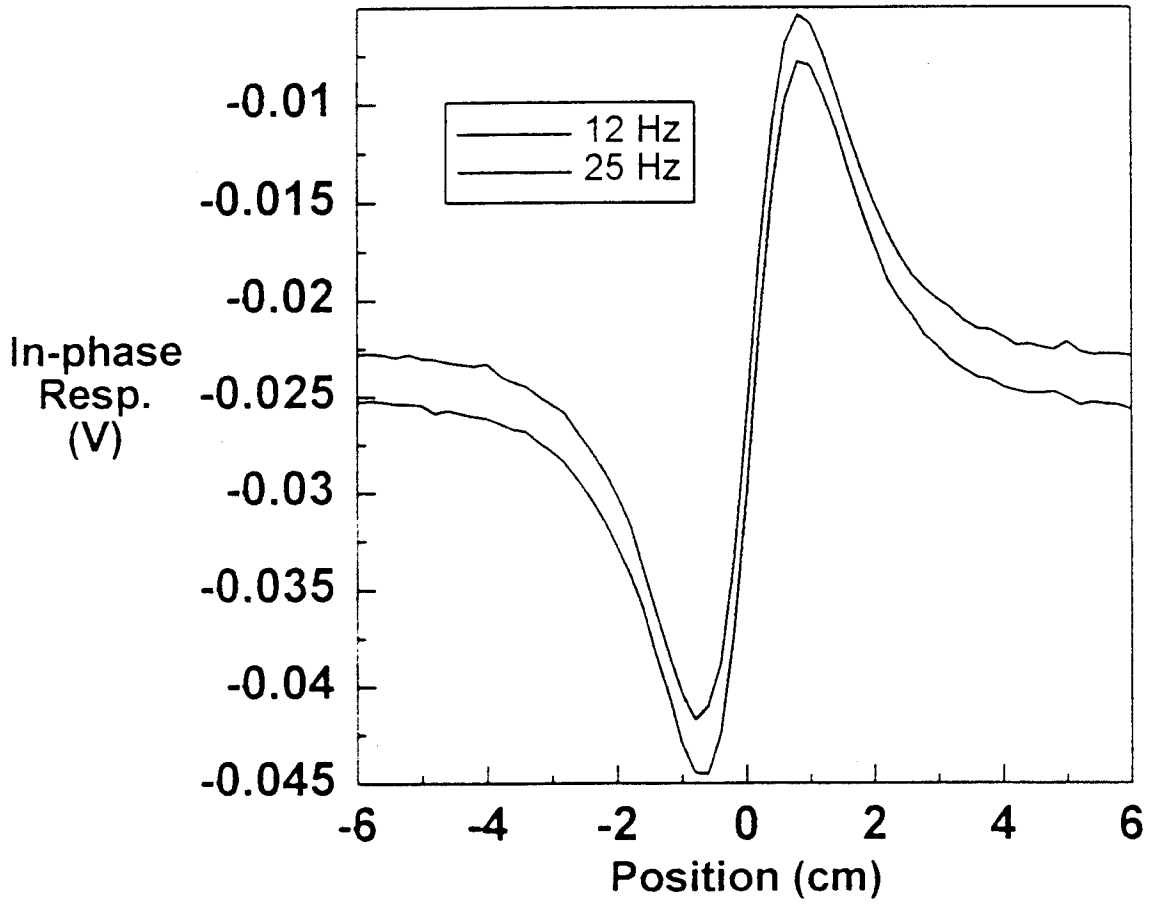

Figure 43. Comparison of the In-phase responses for 12 and 25 Hz AC currents through Cu wire with a current of 200 micro-amps.

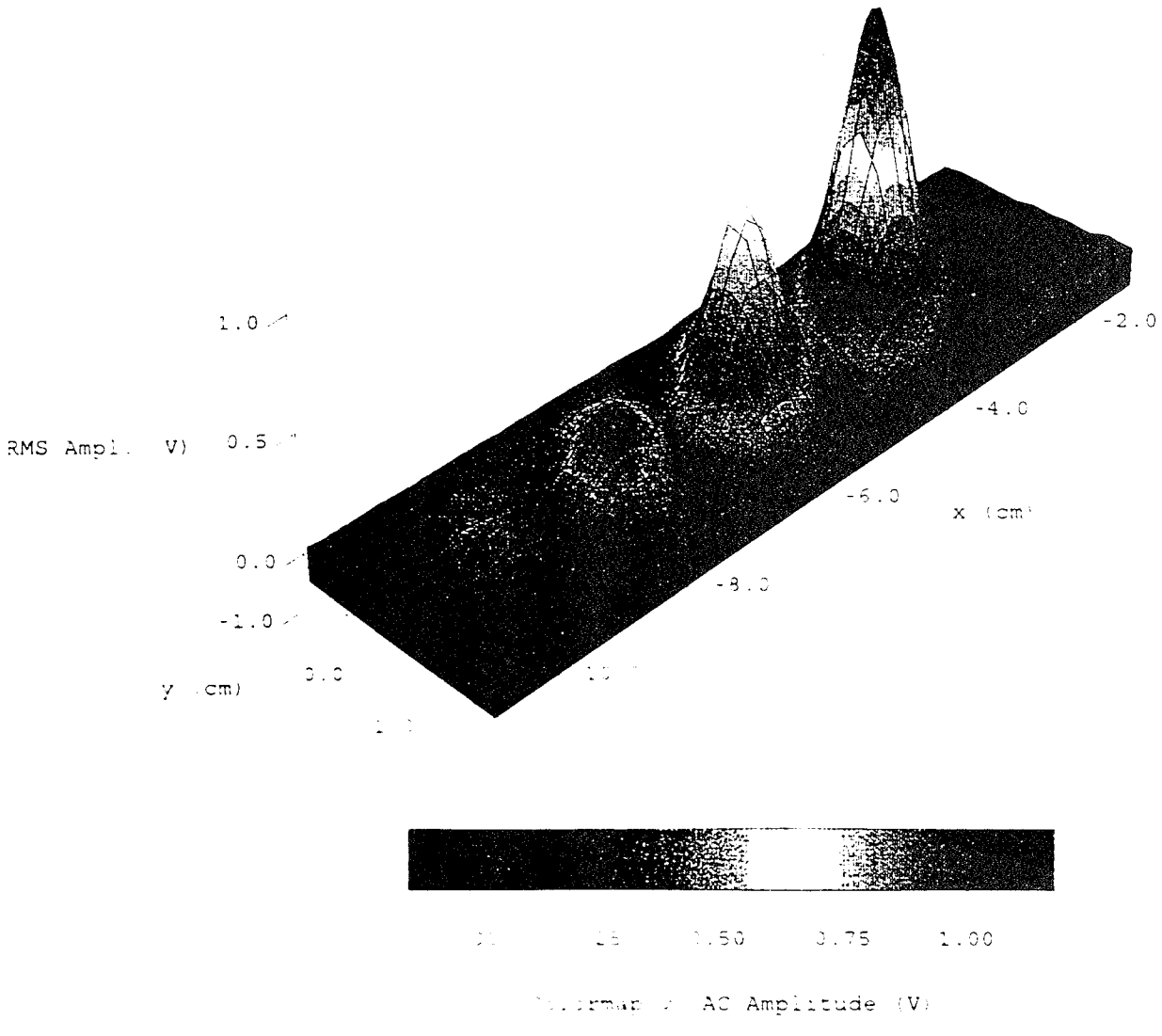

Figure 44. Image of series of holes (as described in text) in a stainless steel plate. The AC magnet current is 5 Amps

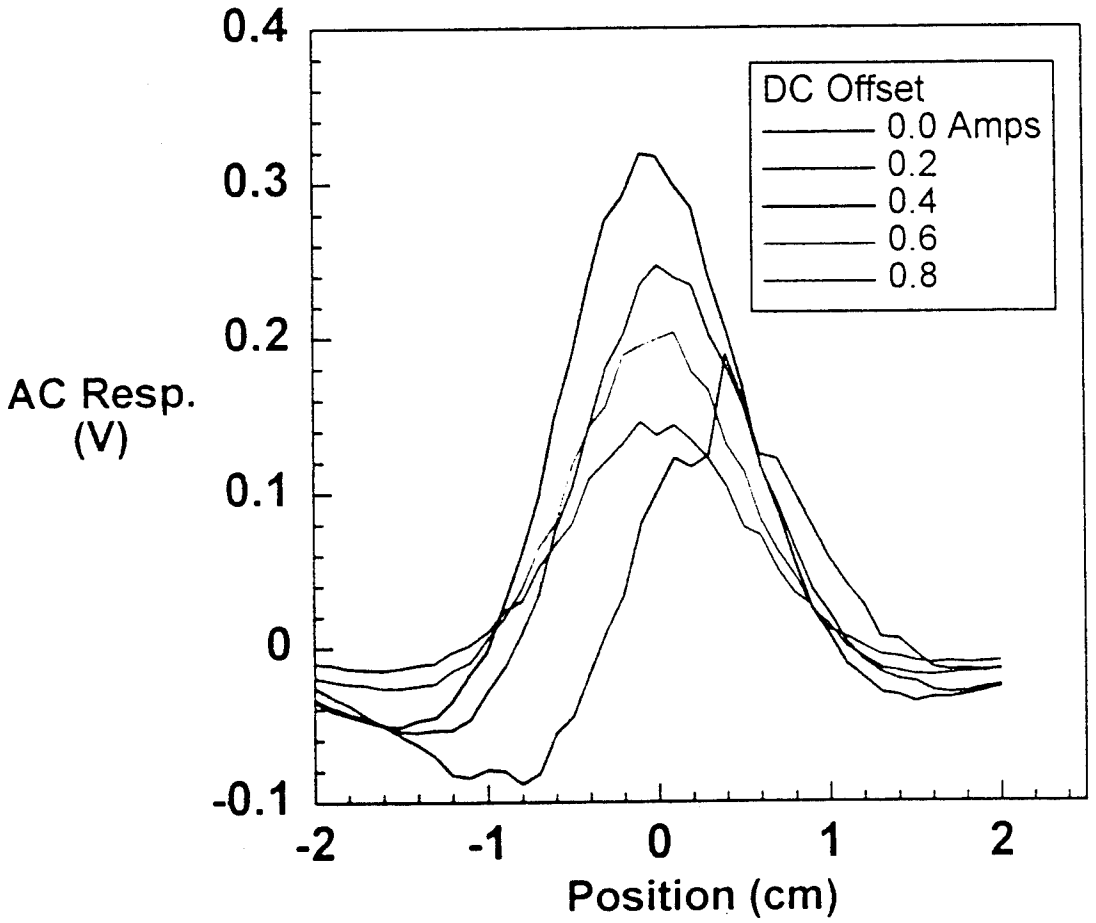

Figure 45. A series of scans across a 0.007" Fe wire under various stressed conditions. A linear motor induces an AC strain (AC current amplitude is 0.2 Amps) with an additional DC offset current as indicated. Thus the response is a measure of the derivative (wrt the applied stress) of the magnetization change. It is observed that the peak heights increase with offset current, then reverse and begin to decrease.

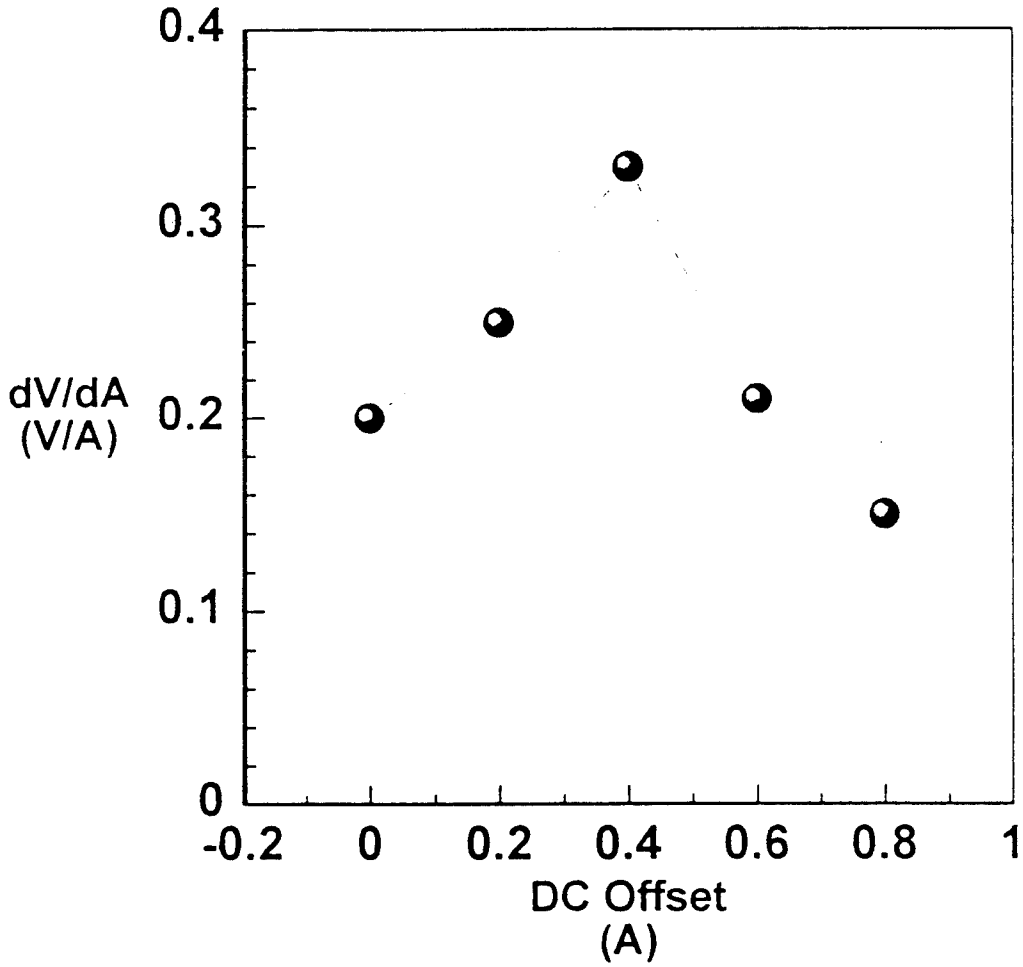

Figure 46. The peak heights from previous figure plotted as a function of offset current. The peak may be related to the Villari reversal, but it is important to understand that the measurements here are not magnetization vs. tension as would be necessary for demonstration of either magnetostriction or the Villari effect. This does show the techniques that may be employed in the investigation of magnetostrictive effects, and the potential for NDE studies.

3. Publications

4. Professional Personnel Associated with the Research Effort

Dr. Douglas Paulson, Principal Investigator
Ph.D. Physics, University of California at San Diego, 1974.
Dr. Paulson has designed and developed many SQUID-based magnetometer systems and applied them to a wide variety of research topics for more than 25 years.

Dr. Duane Crum
Ph.D. Physics, The Ohio State University 1973
Dr. Crum has managed the design, development, and use of SQUID magnetometers for applications in NDE, geophysics, biomagnetism, physics, and chemistry. Most recently, he was the principal investigator on an EPRI funded grant to use SQUID magnetometers for NDE of metal objects. Many of the techniques and measurement problems are similar to those encountered on this project.

Guy Covert
M.Sc. Electrical Engineering, California State University, San Diego, 1972
Mr. Covert has over 22 years experience in electronic design and software development including analog circuit design, microprocessor systems, CAD equipment design, and digital signal processing system design.

Dr. Raymond Sarwinski
Ph.D. Physics, University of Illinois, 1966
Dr. Sarwinski has over 30 years of experience in the design of advanced cryogenic systems for applications in the military and commercial sectors. His specialties are magnet design, magnetometer design, theoretical analysis, ultra-high sensitive instrumentation, and the design of closed-cycle refrigeration systems.

John Peter Wikswo, Jr.
MOS. and Ph.D. - Physics, Stanford University, 1973
Appointments
Research Fellow in Cardiology, Stanford University School of Medicine 1975-1977
Assistant Professor of Physics, Vanderbilt University 1977-1982
Associate Professor of Physics, Vanderbilt University 1982-1988
Professor of Physics, Vanderbilt University 1988-AMB. Learned Professor of Living State Physics (effective September 1991)

5. Interactions

We have had significant interactions with Dr. Bruce Westermo of Strain Monitor Systems. In addition to provided us with strained samples as discussed above, we have had discussions regarding the feasibility of incorporating an NDE system as a method of detecting induced strain in structures where critical access may be limited. Both development of the strain monitor and optimal signal detection methods would be required.

The following individuals were expected to have some interest in this type of magnetometer for NDE purposes. We have not been able conduct meaningful discussions with them at this point to ascertain their interest in the NDE system for investigation of specific areas:

N/A

• Steve Baughman	Lockheed, Marietta, GA	(C-141 and C-5A)
• T. M. Cordell	Wright Patterson AFB Branch Chief, NDE Branch Materials Directorate, Wright Lab.	
• Richard Kinsey	Air Force Corrosion Program Warner Robins AFB	
• Donald Hazen	Warner Robins Air Logistics Center	
• David Raulerson	Pratt and Whitney	
• Various personnel	McDonnel Douglas	(F-15)
• Crawford Battle	F-15 Program Depot Maintenance Warner-Robbins AFB	
• Dean Bolton & Staff	Sacramento Air Logistics Center McClellan AFB	
• Leon Yeager	Hill AFB	(F-4)
• Capt. Bullock	Hill AFB	(F-16)
• Hugh Nelson	Warner Robbins AFB	(C-130)
• Clarence Hitchings	San Antonio Air Logistics Center	(C-5)

All of the personnel who have been contacted thus far have indicated a willingness to provide additional information in support of this effort.

6. New Discoveries, Inventions, Patent Disclosures and Applications.

None identified or applied for as yet.

7. Additional Statements

None.